# Thermal Memory in Self-Assembled Collagen Fibril Networks

Martijn de Wild, Wim Pomp, and Gijsje H. Koenderink*
Biological Soft Matter Group, FOM Institute AMOLF, Amsterdam, the Netherlands

ABSTRACT Collagen fibrils form extracellular networks that regulate cell functions and provide mechanical strength to tissues. Collagen fibrillogenesis is an entropy-driven process promoted by warming and reversed by cooling. Here, we investigate the influence of noncovalent interactions mediated by the collagen triple helix on fibril stability. We measure the kinetics of cold-induced disassembly of fibrils formed from purified collagen I using turbimetry, probe the fibril morphology by atomic force microscopy, and measure the network connectivity by confocal microscopy and rheometry. We demonstrate that collagen fibrils disassemble by subunit release from their sides as well as their ends, with complex kinetics involving an initial fast release followed by a slow release. Surprisingly, the fibrils are gradually stabilized over time, leading to thermal memory. This dynamic stabilization may reflect structural plasticity of the collagen fibrils arising from their complex structure. In addition, we propose that the polymeric nature of collagen monomers may lead to slow kinetics of subunit desorption from the fibril surface. Dynamic stabilization of fibrils may be relevant in the initial stages of collagen assembly during embryogenesis, fibrosis, and wound healing. Moreover, our results are relevant for tissue repair and drug delivery applications, where it is crucial to control fibril stability.

## INTRODUCTION

Collagens are the most abundant structural proteins in the extracellular matrix of vertebrates. They form filamentous frameworks that provide mechanical strength to connective tissues such as tendon, skin, and bone (1). Moreover, collagen plays a key role in the regulation of important cell functions such as migration and differentiation (2). The main fibril-forming collagen in mammals is type I collagen, which consists of two identical $\alpha$1(I) chains and a $\alpha$2(I) chain intertwined into a rod-like triple helix. In vivo, collagen self-assembles into fibrils upon enzymatic conversion of soluble procollagen precursors into insoluble tropocollagen monomers (3). Tropocollagen has a triple helical region of ~1000 amino acid residues flanked on both sides by short, nonhelical regions known as the N- and C-telopeptides (Fig. 1 *A*, see figure caption for definition of *length scales*). The monomers are very long (300 nm) and thin (1.5 nm) and behave in solution as flexible polymers with a persistence length of ~10 nm (4,5) (Fig. 1 *B*). They self-assemble into supramolecular fibrils with a precise axial stagger between neighbors of 67 nm, known as the D-period (6) (Fig. 1, *C* and *D*). Because each molecule spans a nonintegral number of periods (4.46 D), each period contains an overlap and a gap region that cause a cross-striated appearance in electron micrographs (Fig. 1 *E*). The D-banded axial periodicity is essential to ensure a high tensile strength (7,8), to regulate cellular recognition and binding of extracellular matrix molecules (9), and to template bone mineralization (10). Accordingly, mutations in type I collagen that cause defects in assembly are associated with severe connective tissue disorders (11).

In vitro assembly studies have provided key insights into the mechanism by which D-staggered collagen fibrils form. It was shown early on that purified collagen can form fibrils with the same axial periodicity as native fibrils without any accessory extracellular matrix components (12). Similar to native fibrils, the fibrils are tens of micrometers in length and ~100 nm in diameter (13). Thus, all the required structural information is encoded in the primary sequence. The kinetics of fibril assembly has been studied extensively, usually by measuring the increase in solution turbidity that accompanies fibril formation. Turbidimetric growth curves of collagen exhibit an initial lag phase, followed by a growth phase during which the turbidity increases in a sigmoidal fashion (13–16). This behavior is characteristic of a cooperative nucleation and growth mechanism. However, uncertainty remains about the exact nature of the nucleus and the degree of cooperativity (17–21) and about the mechanism of growth (22–25). There is some evidence that five-stranded microfibrils are already formed during the turbidimetric lag phase, which subsequently grow linearly and laterally during the growth phase (16,18). Several studies indicate that collagen monomers undergo conformational changes during the lag phase (23,26–28). Indeed, tropocollagen has to convert from a fluctuating, coiled conformation in solution (Fig. 1 *B*) to a straightened conformation inside fibrils (Fig. 1 *C*).

Collagen assembly is driven by noncovalent interactions, which are reversible upon changes in temperature or solution conditions. Assembly is promoted by warming and reversed by cooling, and is thus an endothermic process, similar to the assembly of other biopolymers such as actin and microtubules (29,30) and opposite to typical synthetic supramolecular materials (31). Assembly is thus driven by an increase in

*Submitted December 17, 2012, and accepted for publication May 10, 2013.*

*Correspondence: g.koenderink@amolf.nl

Wim Pomp's present address is Leiden Institute of Physics, Leiden University, Niels Bohrweg 2, 2333 CA Leiden, the Netherlands.

Editor: Enrique De La Cruz.



0006-3495/13/07/0200/11 $2.00

http://dx.doi.org/10.1016/j.bpj.2013.05.035

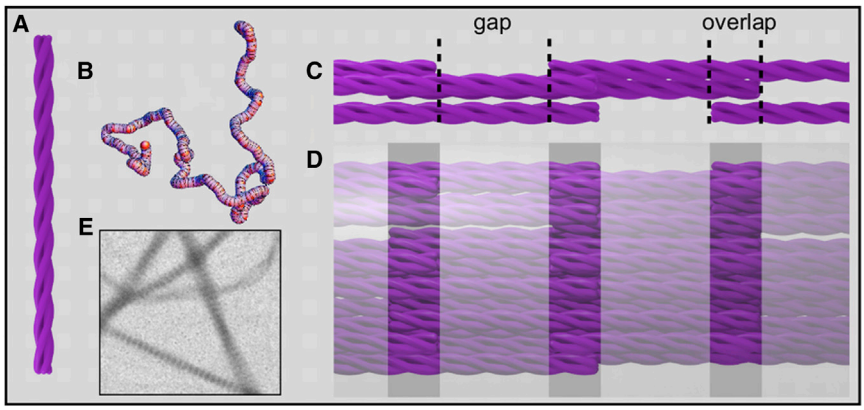


FIGURE 1 (*color online*) Schematic representation of the hierarchical self-assembly of type I collagen. (*A*) Collagen molecules consist of three polypeptide chains twisted into a rod-like triple helix (not shown to scale; in reality the length is 300 and the diameter 1.5 nm). (*B*) The monomers are flexible polymers with a persistence length of ~10 nm. Shown is a typical conformation obtained by Monte Carlo simulations (courtesy of H. Amuasi). (*C*) Pentameric aggregate of collagen monomers in a D-staggered parallel arrangement. Note the straightened conformation of the collagen molecules. Each tropocollagen spans 4.46 D periods, giving rise to an overlap and a gap region within each period. (*D*) Fibrils are constructed from many pentamers. (*E*) Transmission electron micrograph (2 $\mu$m wide) of negatively stained collagen fibrils assembled at 37°C in a physiological buffer clearly shows D-banding with an axial periodicity of 67 nm.

entropy, resulting from the release of water molecules from the surface of tropocollagen helices (32). Opinions differ as to the relative contribution of different classes of noncovalent interactions to the thermodynamic driving force for assembly. Hydrophobic interactions are likely to play an important role. Atomistic simulations showed that water molecules are released from hydrophobic amino acid residues when the molecules pack into a fibril (33). Moreover, analysis of the amino acid sequence of collagen showed that hydrophobic residues occur in clusters and that D-staggered packing optimizes the alignment of hydrophobic side chains between apposing tropocollagens (34,35). Yet, there is also an alternative interpretation of the endothermic nature of collagen assembly, namely that water is released from polar residues. According to this interpretation, the dominant driving force is provided by hydration forces associated with water-mediated hydrogen bonding between polar residues (36–38). This interpretation is supported by observations that sugars and polyols strongly reduce the attraction between collagen helices and suppress fibrillogenesis (19,39,40). These compounds are expected to disrupt water-mediated as well as direct hydrogen bonding between polar residues. Recent simulations indeed indicate that clusters of hydrogen-bonded water exist in collagen fibrils, but the relative importance of hydration forces and hydrophobic forces could not be determined (33). The dependence of fibril assembly on solution pH and ionic strength suggests that electrostatic interactions also reinforce the stability and/or axial specificity of assembly (20,41,42). The D-staggered packing arrangement appears to optimize alignment between complementary charges on opposing helices (34). Some studies also implicate specific ions such as divalent phosphate in providing salt bridges and improving axial order (15,42,43). Finally, there is evidence that the telopeptides further enhance the specificity of molecular recognition (44). When the telopeptides are removed by pepsin or other proteases, nucleation is slowed down and the activation energy is increased (45–47). Computational models show that telopeptides dock to specific helix recognition sites and induce reciprocal conformational changes (48,49). It remains unknown whether this interaction is only catalytic in the initial stages of assembly or contributes also to the driving force.

Despite several decades of intensive research on the process of collagen assembly, the molecular basis of the interactions responsible for collagen fibril stability (and mechanical strength) remains poorly understood. Here, we take an alternative approach to elucidate the role of noncovalent interactions mediated by the collagen triple helix in fibrillogenesis. Rather than studying the process of assembly, we focus on the kinetics of cold-induced fibril disassembly. As a model system, we use collagen whose telopeptides are removed by pepsin. This is necessary to prevent spontaneous formation of intermolecular covalent cross-links (17,46,50–52). We used several complementary methods to characterize the kinetics of cold-induced disassembly of collagen fibrils formed at body temperature (37°C): we used turbimetry to probe the fraction of collagen in fibril form, atomic force microscopy (AFM) to probe the fibril morphology, and confocal microscopy and rheometry to measure the network connectivity. We demonstrate that collagen fibrils disassemble by subunit release from their sides as well as their ends, with complex kinetics involving an initial fast release followed by a slow release. Despite the absence of telopeptides, the fibrils are gradually stabilized over time. This dynamic stabilization may reflect structural plasticity of the collagen fibrils arising from their complex structure. In addition, we propose that the polymeric nature of collagen monomers may lead to slow kinetics of subunit desorption from the fibril surface. Dynamic stabilization of fibrils may be relevant in the initial stages of collagen assembly in vivo (2).

## MATERIALS AND METHODS

### Preparation of collagen gels

Bovine dermal collagen I (NUTRAGEN) was purchased as a 6.0 mg/ml solution in 0.01 M HCl from Advanced Biomatrix (San Diego, CA). This collagen is isolated from bovine hides by enzymatic digestion with pepsin,

which removes portions from the N- and C-terminal telopeptides containing the lysine groups that are responsible for intermolecular cross-linking in vivo (53). Sodium dodecyl sulfate polyacrylamide gel electrophoresis (SDS-PAGE) on 4% gels was used to assess the purity and degree of intramolecular cross-linking. Gels were stained with Instant Blue Coomassie staining solution (Expedeon, Harston, UK). Samples with a final volume of 500 $\mu$L and collagen concentration of 1 mg/ml were prepared by diluting the stock solution with a buffer mixture, to give a final buffer composition of 10 mM phosphate and 160 mM NaCl at pH 7.2 (I = 0.17). This is a near-physiological buffer that promotes a native D-banding pattern. In the case of turbidity experiments, the buffer mixture was degassed in a vacuum before mixing with collagen, to prevent the formation of air bubbles. All preparation steps involving collagen were performed at 4°C. Unless otherwise noted, chemicals were purchased from Sigma Aldrich (St. Louis, MO). The extent of collagen polymerization at 37°C was tested by precipitating the fibrils by centrifugation for 10 min at 16,100 $\times$ $g$ in a 5415R tabletop centrifuge (Eppendorf, Hamburg, Germany) at 37°C. The collagen concentration in the supernatant was measured using the sirius red assay (54). The supernatant (100 $\mu$l) was incubated for 30 min with 1 ml of 1 mg/ml Direct Red 80 in 1% picric acid. The solution was centrifuged for 10 min at 16,100 $\times$ $g$, the supernatant was removed, and the pellet was washed (to remove excess dye) with 750 $\mu$l of 0.01M HCl. The pellet was finally dissolved in 250 $\mu$l 0.5M NaOH. After 5 min, the solution absorbance at 550 nm was measured using a Nanodrop 2000 spectrophotometer (Thermo Scientific, Waltham, MA) and calibrated against stock collagen in the same buffer.

## Turbidity measurements

The kinetics of collagen polymerization at 37°C and subsequent depolymerization induced by cooling were probed by measuring the change in solution absorbance at a wavelength of 370 nm ($A_{370}$) with a Lambda 35 dual-beam spectrophotometer (PerkinElmer, Waltham, MA) equipped with a PTP 6+6 Peltier temperature controller. Solutions of 1 mg/ml collagen were pipetted into a quartz cuvette (Quartz Suprasil precision cells 115B-S, Hellma Analytics, Mullheim, Germany) equilibrated to 37°C and absorbance readings were initiated within 15 s. The baseline value was taken as the first recorded turbidity value. The absorbance readings were converted into turbidity values, $\tau$, by using the relation $\tau = (A_{370} \ln (10))/L$, where $L$ is the optical path length (1.0 cm). It was previously shown by comparison with fibril precipitation experiments that the turbidity of collagen solutions is directly proportional to the amount of mass present in fibril form (13,15). Thus, the turbidity provides a reliable, and model-independent, measure of the relative degree of polymerization as a function of temperature. In some experiments we measured the wavelength dependence of the turbidity with 2 min time intervals; using light scattering theory modeling the fibers as rigid rods (55,56) it is possible to infer the fibril diameter and mass-length ratio (see the Supporting Material Note S1 and Fig. S1). Collagen fibrils were always first allowed to assemble for 2 h at 37°C, and the absorbance was recorded with 30 s intervals. Subsequently, fibril disassembly was induced by lowering the temperature to target values between 4 and 37°C. We used two different disassembly protocols: temperature step experiments and temperature ramp experiments. The actual time needed for the sample to reach a given target temperature in step experiments varied from 1 to 4 min, depending on the target temperature, as measured with a thermocouple. In temperature ramp experiments, the temperature was lowered at a constant rate between 0.2 and 129°C/h. The actual time dependence of the temperature was measured with a thermocouple and used in the analysis. The solution absorbance during disassembly was measured for 2 h at 30 s intervals in step experiments and at 15 min intervals during ramp experiments.

## AFM and transmission electron microscopy (TEM)

To characterize fibril morphology and diameter, we imaged fibrils deposited on Formvar-coated glass coverslips using AFM (Dimension 3100 AFM, Veeco digital instruments, Plainview, NY). We were unable to image the fibrils in buffer, because the fibrils are very soft and easily pollute the AFM tip or dislodge from the surface. For this reason, we imaged the fibrils in air. For comparison, we also performed TEM at 80kV (Tecnai G2, FEI company, Hillsboro, OR) on samples that were prepared identically, but on Formvar-coated copper electron microscopy (EM)-grids. The glass substrates for AFM were cleaned with 70% ethanol and dried with a flow of $N_2$, and then briefly dipped into a Formvar solution (1% in 1,2-dichloroethane) and slowly extracted to ensure a homogeneous layer. The Formvar was allowed to dry in air. The substrate was placed gently for 10 s on top of a collagen gel (polymerized in a humified petri dish) at the appropriate temperature. The substrate was washed 3 times with phosphate buffered saline (PBS) of pH 7.2 and 3 times with milliQ, water to prevent the formation of salt crystals. All solutions were of the appropriate temperature and excess liquid was blotted off with filter paper after each washing step. The substrate was dried at 37°C for at least 2 h. The fibrils were imaged in tapping mode using a TESPA doped silicon cantilever (Bruker AXS, Camarillo, CA) with a nominal tip radius of 8 nm and spring constant of 42 N/m. Images were flattened using the Nanoscope software (6.14R1, Veeco digital instruments), but otherwise unaltered. The fibril width and height were analyzed in ImageJ software (version 1.46a, National Institutes of Health, Bethesda, MD), averaging over 20 fibrils per experimental condition.

## Confocal reflectance microscopy

The three-dimensional architecture of collagen gels in their native, hydrated state was examined by confocal microscopy with an Eclipse Ti inverted microscope (Nikon instruments Europe, Amstelveen, The Netherlands). We used the reflectance mode, to avoid the use of fluorescent labels, which can influence collagen (de)polymerization (57–59), using 457 nm light from an Ar laser (Melles Griot, Albuquerque, NM). Collagen gels were polymerized for 2 h at 37°C in glass chambers made from a microscope slide and coverslip separated by Parafilm spacers and sealed with vacuum grease. Gels were imaged either directly after polymerization or after subsequent cooling to 4°C. Image stacks were obtained at least 10 $\mu$m away from the glass surface by scanning through the $z$ direction in steps of 0.5 $\mu$m over a range of 20 $\mu$m with a piezo-driven 100$\times$ oil immersion objective (Nikon). To optimize the signal/noise ratio, we used 2$\times$ line average. Maximum intensity $z$ projections were made with ImageJ.

## Cone-plate rheology

The linear viscoelastic properties of the collagen gels were measured using a stress-controlled MCR501 rheometer (Anton Paar, Graz, Austria) with a CP40-2 acrylic measuring cone with 40 mm diameter and 2° angle and a steel bottom plate heated to 37°C with a PTD200 Peltier system. The collagen solution was applied to the prewarmed rheometer, and allowed to polymerize in situ for 2 h before starting oscillatory shear measurements. The sample was in a closed hood to maintain a constant temperature and humidity. The frequency-dependent shear modulus $G^*(\omega) = \sigma(\omega)/\gamma(\omega)$ of the collagen gels was measured by applying an oscillatory strain $\gamma(\omega)$ decreasing logarithmically from 34 to 0.0628 rad/s, and recording the stress response, $\sigma(\omega)$. The strain amplitude was 0.5%, which is much smaller than the critical strain (~5%) where nonlinearity sets in. $G^*(\omega)$ is a complex modulus with an in-phase (elastic) component, $G'(\omega)$, and an out-of-phase (viscous) component, $G''(\omega)$.

# RESULTS

## Kinetics of collagen assembly and disassembly

Collagen self-assembly is entropy-driven and depends on noncovalent interactions (20,32). Fibrils can be assembled

by heating a collagen solution from 4 to 37°C and disassembled by subsequent cooling. We use turbidimetry to analyze the kinetics of the disassembly process in response to a sudden stepwise lowering of the temperature, because the solution turbidity is a direct measure of the amount of mass present in fibril form (13,15). Fig. 2 *a* shows three typical assembly-disassembly experiments, with identical assembly conditions (1 mg/ml collagen in PBS, 2 h at 37°C) but differing in disassembly temperature ($T_{dis}$ = 4, 17, 27°C). The change in turbidity during the assembly phase is highly reproducible, showing three distinct phases characteristic of a nucleation-and-growth process (14). There is an initial lag phase of ~10 min with no turbidity change. Prior studies indicate that short, thin fibrils are already present at the end of the turbidimetric growth phase with ~100 collagen molecules per unit length, but the structures are too small during the lag phase to give a measurable turbidity (16,22,60). This is confirmed by our own wavelength-dependent turbidity measurements (Note S1 and Fig. S2 *a*). The lag phase is followed by a growth phase with a sigmoidal increase in turbidity, during which the collagen fibrils grow in length and width. Wavelength-dependent turbidity data show that the mass-length ratio of the fibrils also increases sigmoidally during the growth phase (Fig. S2 *a*). Finally, all three turbidity curves reach a plateau phase where the turbidity reaches a constant level (2.57 ± 0.06), which varies by <4% among experiments. It actually takes 6 h for the turbidity to reach a constant value, and at 2 h, the turbidity has reached ~93% of this maximum (consistent with precipitation experiments, showing that collagen assembly after 2 h is 87% complete). Nevertheless, for practical reasons we always assemble gels for only 2 h, and denote the fibrils at this point as mature, with a turbidity value $\tau_{37}$. Wavelength-dependent turbidity data indicate that the mature fibers have an average diameter of 61 nm (Fig. S2 *b*) with 1070 monomers per cross section (Note S1), consistent with prior reports for rat tail collagen (61).

After 2 h, we reduce the temperature stepwise, which causes an immediate drop in the turbidity (Fig. 2 *A*). The slope of the turbidity response curve is relatively shallow in the first few minutes, because of the finite duration of the temperature step (1–4 minutes). The turbidity value $\tau_{dis}$ reached after 2 h of disassembly is strongly dependent on the disassembly temperature: the lower the temperature, the lower $\tau_{dis}$, indicating that the fibrils release more mass. The kinetics of disassembly clearly does not follow a simple single exponential form. Empirically, the decay curves are well fit by a sum of two exponentials, corresponding to a fast decay with a characteristic decay time of ~9 min, independent of disassembly temperature, followed by a slow decay with a decay time that increases from 200 min at 4°C to 2000 min at 27°C (Fig. S3). At 32°C, the turbidity is essentially constant at long times. As shown in Fig. S4, the turbidity during a disassembly experiment at 22°C is actually still not constant after 4 days.

To quantify the extent of disassembly, we take the ratio between the turbidity measured after disassembly and that measured for the mature fibrils, $\tau_{dis}/\tau_{37}$, which is a measure of the degree of fibril stability. For practical reasons, we measure this ratio after 2 h of disassembly. Although the disassembly process is <80% complete at this time (Fig. S4), the rate of disassembly is already much smaller than directly after the temperature step, making this an acceptable choice. As shown in Fig. 2 *B*, $\tau_{dis}/\tau_{37}$ decreases nearly linearly when the disassembly temperature is lowered from 32 to 7°C. The turbidity does not return to zero upon cooling, even to 4°C, which indicates that the collagen fibrils do not completely disassemble. To test whether collagen fibrils indeed remain in solution, we cycle samples cooled down to 22°C for 2 h back to 37°C. As shown in Fig. S5, disassembly is reversible, because heating to 37°C brings the turbidity back to its original value. Strikingly, there is no lag phase during the reassembly process, which strongly indicates that collagen fibrils indeed remain and can act as templates for fibril growth upon reheating. The wavelength dependence of the turbidity indicates that fibrils disassembled for 2 h at 4°C still contain 229 monomers per cross section, which is ~20% of the mass/length ratio of mature fibrils (Fig. S2 *a*). The loss in mass from the sides ($\mu_{dis}/\mu_{37}$) is comparable to the overall loss in fibril mass ($\tau_{dis}/\tau_{37}$) at all disassembly temperatures (Fig. S6), suggesting that fibrils predominantly shed monomers from their sides.

The apparent stability of the fibrils at 4°C is surprising, because collagen solutions kept at 4°C and never exposed

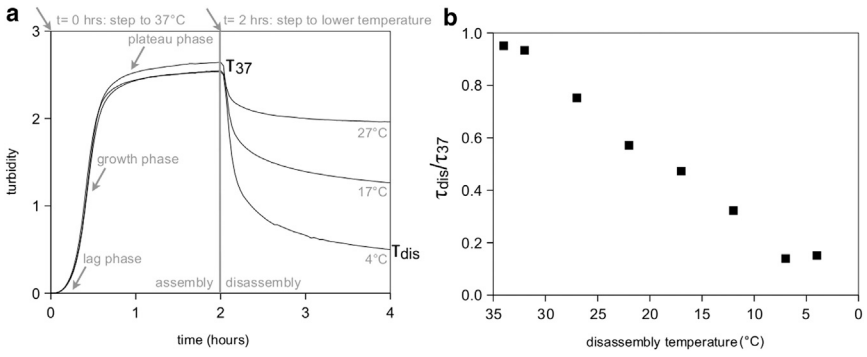


FIGURE 2 Turbidity measurement of the assembly and disassembly kinetics of a 1 mg/ml collagen solution. (*a*) Turbidity response for three collagen samples, each assembled for 2 h at 37°C and disassembled by cooling to different temperatures, $T_{dis}$. (*b*) Temperature dependence of $\tau_{dis}/\tau_{37}$ (note the *inverted temperature axis*).

to 37°C do not develop any measurable turbidity (Fig. S7). This history dependence suggests that fibrils formed at 37°C and cooled to 4°C are kinetically stabilized. It should be noted that, although a collagen solution at 4°C does not produce aggregates detectable by the turbidity method, some aggregation does take place at 4°C. When a neutralized collagen solution is heated to 37°C after 17 h incubation at 4°C, the resulting turbidity curve has no lag phase (*inset* of Fig. S7). Apparently, there is a nonzero driving force for collagen to self-assemble at 4°C into structures that can act as nuclei for fibril growth. The rate of assembly after 17 h incubation at 4°C is slower than the rate of assembly of a freshly neutralized collagen solution (cf. Fig. 2 *A*), suggesting that the oligomeric structures formed at 4°C are different from the aggregates formed in the nucleation phase at 37°C. We conclude that there is a clear history dependence of the turbidity measured at 4°C, suggestive of kinetic stabilization.

To test whether the stability of collagen fibrils at low temperature is truly kinetic in origin, we examined whether collagen gels could be redissolved in 0.01 M HCl. Under these conditions, there is no driving force for collagen fibrillogenesis (62). We polymerize collagen at 1 mg/ml for 2 h and then dialyze against 0.01M HCl at 4°C. To test whether fibril disassembly is complete, we perform an assembly experiment at 37°C with the dialyzed solution. If the fibrils were fully dissolved, the assembly process should have a lag phase, similar to the first assembly step in Fig. S5. However, if parts of fibrils or other nuclei remain because they are being held together by covalent cross-links, there should be no lag phase. For the assembly experiment we use a concentration around 0.1 mg/ml, where the lag phase is longer and easier to recognize than at 1 mg/ml (13). We indeed find that the lag phase returns (Fig. S8), which implies that the collagen fibrils are in principle fully soluble. This indicates that there is some kinetic mechanism that stabilizes the fibrils in a near-physiological buffer at neutral pH. Moreover, this stabilization is apparently an intrinsic property of the collagen triple helix, because we use pepsin-treated collagen that lacks the telopeptides.

## Rate dependence of fibril disassembly

The experiments described previously show the response of the system to an abrupt change of temperature. This is a nonequilibrium experiment, because the temperature is changed much faster than the equilibration time of fibril disassembly. To obtain more insight into the fibrils' equilibration behavior, we perform a series of experiments where the temperature is lowered from 37 to 22°C at a constant rate. Because the temperature jump experiments show a fast disassembly process with a decay time of 9 min and a slow process with a time constant of several days, we choose a range of cooling rates from 0.2°C/h (which takes over 3 days) to 128.6°C/h (which takes 7 min). Fig. 3 shows a typical turbidity response curve, which encompasses three stages, as indicated by the dotted line showing the temperature: 1), assembly for 2 h at 37°C, 2), temperature ramp down to 22°C with a constant rate, and 3), a tail stage at a constant temperature of 22°C. In the assembly stage, fibrils are formed, producing a sigmoidal increase in turbidity. Next, the temperature is ramped down toward 22°C at a rate of 5°C/h. This does not lead to an immediate change in $\tau/\tau_{37}$, likely because the fibrils are not yet fully assembled after 2 h, and continue to grow as long as the temperature is sufficiently close to 37°C. After a short delay, though, $\tau/\tau_{37}$ drops at a constant rate until the target temperature is reached. Strikingly, $\tau/\tau_{37}$ continues to decrease at 22°C, at a rate that gradually slows with time. We call this stage the tail stage.

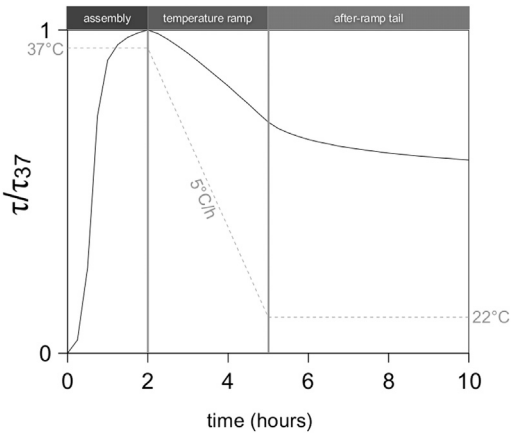


FIGURE 3 Normalized turbidity response ($\tau/\tau_{37}$) of a 1 mg/ml collagen solution during a temperature ramp experiment. There are three stages, as indicated by the dotted line showing the temperature: 1), an assembly stage for 2 h at 37°C, 2), a temperature ramp stage in which the temperature is lowered to 22°C at a constant rate, and 3), a tail stage, during which the temperature is maintained at 22°C.

Remarkably, the fibrils' response during the temperature ramp stage is independent of the cooling rate within experimental error (Fig. 4). Note that, because the sampling rate is limited to one measurement every 15 min, the faster ramps have only a few data points. Nevertheless, these data clearly show that $\tau/\tau_{37}$ is a function of the temperature alone, and not of the rate of change of the temperature. This is true for a broad range of ramp rates, with the fastest rate being over 600 times faster than the slowest one. This result suggests that a certain fraction of collagen monomers on the surface of the fibrils is quickly exchangeable. However, this is clearly not true for all monomers, because after the ramp stage, the fibrils continue to disassemble at a slow rate. As shown in Fig. 5 *A*, the extent of disassembly at 22°C depends on the cooling rate of the preceding ramp stage. The higher the cooling rate during the ramp, the larger the decrease of $\tau/\tau_{37}$. The disassembly curves have a complex functional form, which we did not attempt to fit. The initial rate of disassembly, measured as the initial slope of

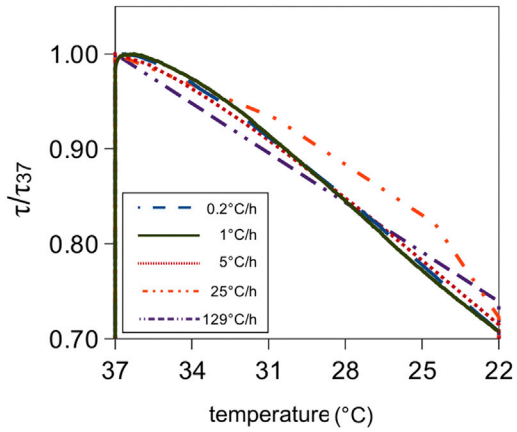


FIGURE 4 (*color online*) Normalized turbidity response ($\tau_{dis}/\tau_{37}$) of five different collagen networks during the temperature ramp stage of temperature ramp experiments. In each case, the temperature is lowered from 37°C to 22°C, but at different rates, as indicated in the legend.

$\tau/\tau_{37}$, increases approximately linearly with the cooling rate (Fig. 5 *B*). This thermal memory effect is strongly suggestive of a slow, time-dependent stabilization of the collagen fibrils: when the fibrils are cooled at a slower rate, there is more time for fibril stabilization. To test this hypothesis, we assemble collagen fibrils at 37°C for various lengths of time and measure the turbidity change in response to abrupt cooling to 22°C. In accordance with our hypothesis, we observe that the apparent stabilization (expressed in terms of $\tau_{dis}/\tau_{37}$) increases from $\tau_{dis}/\tau_{37} = 0.24$ to 0.75 when the incubation time at 37°C is increased from 1 to 18 h (Fig. S9).

## Disassembly causes fibril thinning but leaves the fibril structure intact

Turbidimetry provides an ensemble measure of the degree of fibril disassembly, but gives no information on the changes in fibril morphology or network structure upon cooling. It is conceivable that disassembly might change the packing structure of the fibrils. To directly visualize effects of disassembly on fibril morphology, we use AFM to image collagen fibrils directly after assembly (2 h at 37°C) and after disassembly at either 22 or 4°C for 2 h. As shown in Fig. 6, mature collagen fibrils are long and straight and have an average apparent width of 221 ± 28 nm and height of 30 ± 9.6 nm. This flattening was also observed elsewhere (63), and is most likely a consequence of adsorption to the substrate and (partial) loss of hydration water upon drying in air (64). The measured fibril width and height are therefore not directly representative of the diameter of fibrils in their native, hydrated state. However, we can still use AFM to measure relative differences among different temperature conditions. In most of the fibrils the distinctive 67 nm D-periodic banding is visible, as exemplified by the axial height profile shown underneath the image.

Disassembly at 22 or 4°C for 2 h clearly changes the fibril dimensions. The average apparent width decreases to 175 ± 25 nm at 22°C and 146 ± 34 nm at 4°C, whereas the average height decreases to 22 nm in both cases (± 9 nm at 22°C and ± 4 nm at 4°C). These changes indicate that the fibrils lose mass from their sides, consistent with the reduction of the fibril mass-length ratio measured by wavelength-dependent turbidimetry (Fig. S6). However, the major morphological features are not visibly affected by disassembly. The fibrils still appear long and straight, and retain their D-banding, indicating that the native intermolecular stagger is still intact. The fibrils still appear as flattened cylinders, structurally the same as mature fibrils, which suggests that no large groups of monomers break off during the disassembly process. We conclude that disassembly occurs all along the fibril by dissociation of monomers or small aggregates from the outer surface of the fibril, with the remaining fibril core retaining its structure and organization.

A striking feature of the AFM data is the material in the background. For the mature fibrils there is a small amount of material, consisting of amorphous aggregates. For the partially disassembled fibrils, the background material is more abundant, especially for the fibrils disassembled at 4°C. For fibrils disassembled at 4°C the background material looks fibrillar. However, it is uncertain whether the background material is also present in solution. We cannot rule out that it may result from the AFM sample preparation. The Formvar-coated glass substrate has a high affinity for collagen, and may therefore cause monomers or oligomers to aggregate on the surface (65). Similar aggregates appear

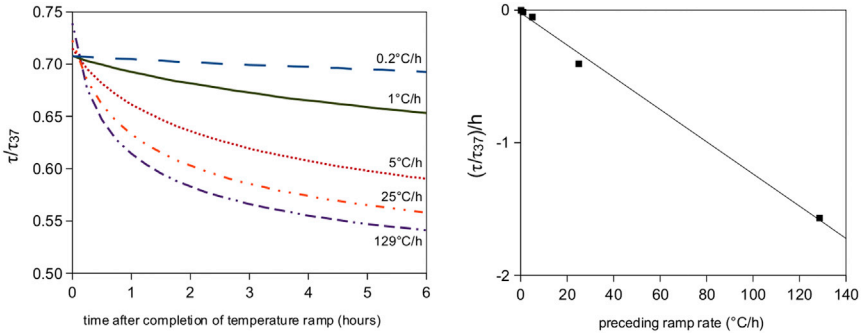


FIGURE 5 (*Left*) Normalized turbidity response ($\tau_{dis}/\tau_{37}$) of five different collagen networks during the tail stage of temperature ramp experiments. For a larger preceding ramp rate, there is more disassembly during the tail stage. (*Right*) The initial slope of each tail response curve is a linear function of the preceding ramp rate.

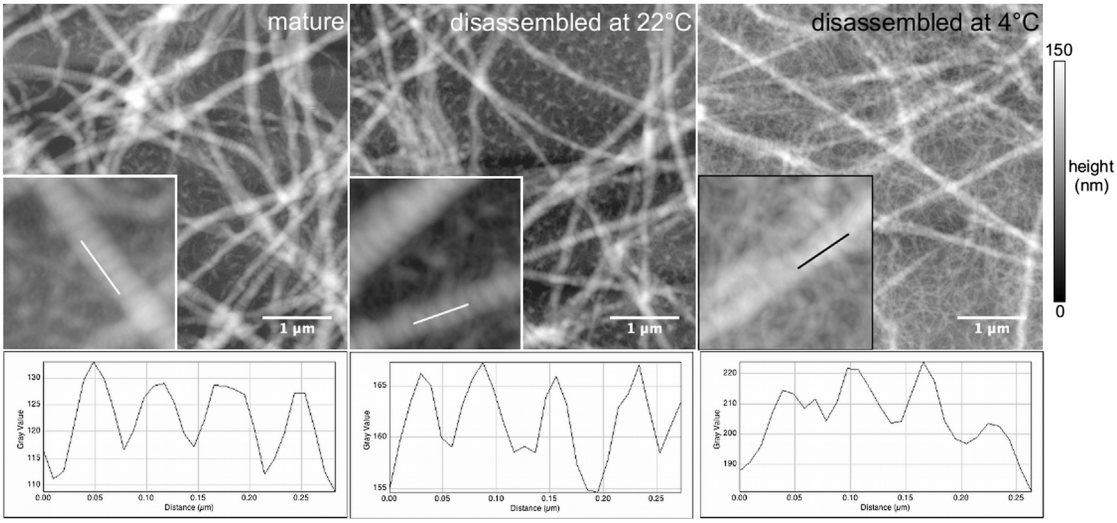


FIGURE 6 Atomic force micrographs of collagen fibrils assembled at 1 mg/ml, (*a*) directly after assembly or after subsequent 2 h disassembly at (*b*) 22°C or (*c*) 4°C. Representative height profiles are measured along a fibril in each image (*white lines in the insets*), showing that the 67 nm D-periodicity is present under all three conditions. Insets (0.78 × 0.78 $\mu m^2$) show an enlarged view of the measured fibrils.

in TEM images of fibrils on Formvar-coated electron microscopy (EM) grids (Fig. S10).

## Disassembly minimally affects network connectivity

The AFM images demonstrate that the turbidity decrease upon cooling is, at least partly, caused by monomer loss from the sides. However, they do not reveal any effects on fibril length because the fibrils are many micrometers long (22). To test whether fibrils also lose mass from their ends, we probe the change in network connectivity at 4°C with two complementary methods. We use confocal reflectance microscopy (CRM) to visualize the networks in their native, hydrated state and reveal their connectivity, homogeneity, and mesh size (57). Moreover, we use cone-plate rheology to measure the elastic modulus of the gels, which is sensitive to network connectivity (66).

Fig. 7 shows two maximum intensity projections of 20 $\mu$m-thick sections of collagen gels, one taken of a gel formed at 37°C for 2 h (*A*) and the other taken after subsequent disassembly at 4°C for 2 h (*B*). At first sight, both images look indistinguishable: the networks are homogeneous and isotropic and have a similar fibril density. In contrast to the AFM images, no change in fibril diameter can be observed. Indeed, the fibrils have diameters below the diffraction limit, so a diameter reduction is only expected to show up in a CRM image when it is so extreme that the fibrils do not backscatter any light. In the mature gel at 37°C, there are no visible fibril ends and also time lapse imaging shows that the fibrils are motionless. Thus, we are unable to determine the lengths of the fibrils. In the gel that has been disassembled at 4°C we can still not recognize fibril ends in still images, but time lapse imaging reveals some dangling fibril ends as recognized by their transverse fluctuations. This effect is illustrated in Fig. 7 *C*, which shows five images with an undulating fibril end in the middle, recorded 4.75 s apart. The position and shape of the fibril in the first frame are marked with five white dots in each frame, which clearly reveals motion of the fibril end. The maximum intensity projection (panel *all*) shows that the fibril end undulates, whereas the other fibrils are motionless. Apparently, there is some endwise shrinkage of filaments. However, the loss in fibril mass

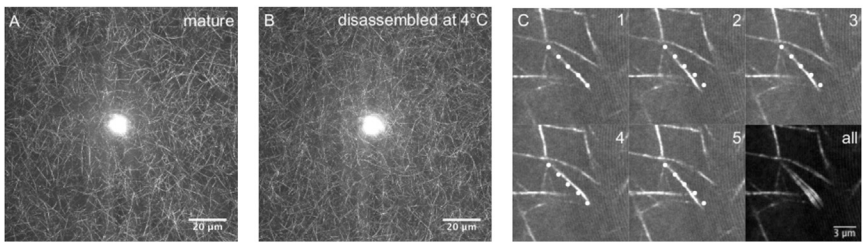


FIGURE 7 Maximum intensity projections of *z*-stacks (41 *z* planes spaced by 0.5 $\mu$m) of a 1 mg/ml collagen gel, (*a*) directly after 2 h of assembly at 37°C, and (*b*) after subsequent disassembly for 2 h at 4°C. The bright spot in the center of the images is an artifact of CRM caused by reflection. (*c*) Five frames of a time lapse movie (taken 4.75 seconds apart) of a 1 mg/ml collagen gel after partial disassembly at 4°C for 2 h. The dotted line indicates a fibril with a dangling end. The last image (*all*) shows a maximum intensity projection that clearly reveals fluctuations of the dangling fibril end.

(85% at 4°C) can clearly not be explained by endwise shrinkage alone, because then we should see only 15% of the original fibril density in the confocal images of disassembled gels. Indeed, the turbidity data show that the overall loss in fibril mass is close to the loss in mass-length ratio (Fig. S6): at 4°C, the overall mass loss relative to mature fibrils is 85%, whereas the loss from the sides is 79%.

To verify that disassembly indeed does not disrupt network connectivity, we also performed rheology on gels before and after disassembly. Fig. 8 shows that after assembly for 2 h at 37°C, the storage modulus, $G'$, is 30 Pa at 1 rad/s, consistent with prior reports (57,66). The gels behave as weak elastic solids, with a slight frequency dependence of $G'$ and a loss tangent $G''/G'$ of 0.25 (*inset*). After subsequent disassembly for 2 h at 4°C, the $G'$ is reduced ~70-fold at an angular frequency of 10 rad/s. However, the sample is still a solid, with an elastic modulus that is only weakly dependent on frequency and a loss tangent that is still below 1 (0.08). Despite losing 85% of its mass, the fibril network remains space-spanning and elastic. The reduction of $G'$ may be caused by the increase in elastically inactive dangling ends observed by confocal microscopy. Prior rheology measurements of collagen networks have shown that $G'$ depends strongly on protein concentration, usually scaling as a power law in concentration with an exponent between 2 and 3 (61,66,67). In addition, the reduction of $G'$ may reflect the reduced fibril rigidity caused by the substantial reduction in fibril diameter. There is not yet a quantitative theoretical model that predicts the modulus of collagen networks. There is evidence that collagen networks deform in a highly nonaffine (nonuniform) manner (68). Nonaffinity is known to make networks much softer than they would be in the affine limit, but there is no quantitative (analytical) prediction of the extent of softening (69). When we reassemble the gel for 2 h at 37°C, $G'$ and $G''$ both return close to their original values. This is in accordance with the turbidity assay showing a return of the original solution turbidity (Fig. S2).

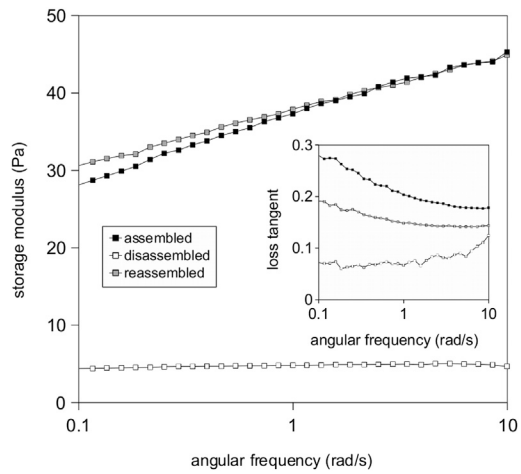


FIGURE 8 Network storage (*elastic*) modulus as a function of angular frequency, for a 1 mg/ml collagen gel subjected to a temperature cycle: fibrils were first assembled for 2 h at 37°C, then cooled down for 2 h at 4°C, and finally reassembled for 2 h at 37°C. The inset shows the corresponding loss tangents.

## DISCUSSION

Prior studies of collagen reversibility focused on covalent stabilization by the telopeptides, which is crucial for the tensile strength of collagen fibrils in vivo. Assembly of neutral-salt soluble or acid-solublized collagen, both of which possess intact telopeptides, is only partly reversible (52,70). Already during polymerization, allysine residues in the telopeptide regions condense with lysine or hydroxylysine residues in helix domains of adjacent molecules in the fibril, creating intermolecular cross-links. Upon aging of collagen gels at 37°C, assembly becomes progressively more irreversible (50,71). When cross-linking is prevented by using lathyritic collagen from animals fed with an inhibitor of lysyl oxidase, assembly is more reversible (72). Yet, there are a few prior turbidimetric reports hinting at a time-dependent increase in stability of fibrils formed from pepsin-collagen (73,74). The buffer composition was different from ours (pH 6.8, 300 mM phosphate), but the observations were comparable. In response to a sudden temperature drop, the turbidity decayed in a biphasic manner and gels aged at 37°C became progressively more insoluble. However, no imaging data were shown, so it is unclear what was the packing arrangement of monomers (which may not be D-staggered at 300 mM phosphate) or the relative contributions of endwise and sidewise disassembly. Similar observations were reported for lathyritic collagen, which also showed thermal memory effects despite the absence of cross-linking (72).

What is the mechanism of the time-dependent stabilization of fibrils? One viable mechanism is structural plasticity. This phenomenon was proposed to cause dynamic stabilization of two other supramolecular protein polymers, actin filaments and microtubules (75,76). Actin filaments, like collagen fibrils, display a biphasic disassembly response and a progressive stabilization upon aging. Based upon EM and x-ray scattering data, it was proposed that filaments can gradually change from a more disordered and unstable structural state into a more ordered and stable structural state. Recently, however, it was proposed that the reported stabilization of actin was due to photo-induced cross-linking induced by the intense illumination employed in the fluorescence microscopy assays used for monitoring disassembly (77). In our study, we robustly find time-dependent stabilization using techniques which do not employ illumination (EM, AFM, rheology). We propose that collagen fibrils may be relatively disordered directly after assembly, but acquire more order over time, by internal rearrangements. It is a formidable challenge, however, to directly demonstrate structural plasticity for collagen fibrils, given their

enormously complex and semicrystalline three-dimensional architecture. While actin filaments and microtubules behave as linear polymers whose assembly dynamics are restricted to the ends, collagen fibrils have hundreds of monomers per cross section packed in an array whose lateral packing order remains poorly understood. Our EM and AFM images indicate that axial order is established immediately, probably because of the high degree of specificity of the noncovalent interactions that drive assembly. However, we have no information on the lateral packing order. X-ray diffraction measurements of native collagen fibrils show varying degrees of lateral disorder (6,78). Fibrils assembled in vitro were shown to have an even less well-ordered lateral packing (12). Synchrotron x-ray scattering measurements or EM microscopy of fibril cross sections may shed more light on time-dependent changes in lateral packing (79). Alternatively, antibodies might be developed that recognize specific structural states of collagen fibrils in analogy to actin and microtubules (80,81). A complementary approach may be computational modeling of collagen fibril assembly using coarse-graining approaches (82), possibly combined with atomistic simulations (5,33).

There are additional complexities in collagen assembly that may contribute to kinetic stabilization of the fibrils. Unlike actin and tubulin monomers, which are compact globular subunits, collagen monomers are long polymers with substantial flexibility (4,5). Both monomer additions to the surface of growing fibrils and monomer removal from disassembling fibrils require large conformational changes of the monomers, which may pose large kinetic barriers. There is indeed some evidence from hydrodynamic assays and vibrational spectroscopy of intramolecular conformational changes during fibril nucleation and growth (23,26–28). A tractable way to model these processes may be by using theories of polymer crystallization and desorption (83–85). Desorption of semiflexible polymers from a surface is known to be slow. Moreover, it is possible that collagen disassembly sets up a complex ecosystem of different supramolecular species that can exchange with the sides and ends of fibrils. For instance, oligomers may be released in addition to monomers and released monomers may potentially associate in solution.

Dynamic stabilization of fibrils may be relevant in the initial stages of collagen assembly in vivo, particularly in growing tissues and during fibrosis and wound healing (2). It will be interesting to test whether other extracellular matrix compounds such as proteoglycans affect the kinetics of cold-induced disassembly of collagen (3). Our results may be of even more direct relevance in the context of biomedical applications. One important area is tissue optical clearing for biomedical optics and photomedicine (86). It is known that the turbidity of biological tissues can be reduced by immersion in chemical agents such as sugar alcohols and restored by immersion in physiological saline. It was proposed that these agents reversibly weaken noncovalent binding forces. Our results may help to explain the basis of this reversibility. A second application area where our results are relevant is in tissue regeneration and drug delivery (87). It is crucial to understand the molecular basis of collagen stability to control the kinetics of in vivo remodeling, resorption, and controlled drug release.

## CONCLUSIONS

We demonstrate that collagen fibrils disassemble by subunit release from their sides as well as their ends, with complex kinetics involving an initial fast release followed by a slow release. Despite the absence of telopeptides, the fibrils are gradually stabilized over time. On a timescale of several days, the fibrils are stable even at temperatures as low as 4°C. Yet, when collagen is never heated and kept at 4°C, there is no formation of fibrils. This is clearly indicative of a kinetic stabilization. Thermal memory is also evident from temperature ramp experiments: when collagen solutions are cooled at a constant rate, the turbidity decreases in a rate-independent manner during cooling, but continues to decrease slowly at a rate that is correlated with the preceding cooling rate once the temperature has reached a constant value. Complementary experiments show that the stability of collagen fibrils formed at 37°C depends on age. We can rule out any irreversible changes such as denaturation, because the fibrils are perfectly soluble in acid and fibrils can be reverted to their original state by reheating to 37°C. We propose that the complex, hierarchical structure of collagen fibrils is responsible for the kinetic stabilization. The dynamic stabilization may reflect structural plasticity of the collagen fibrils arising from their complex structure or slow kinetics of subunit desorption from the fibril surface related to the polymeric nature of the collagen subunits. Dynamic stabilization of fibrils may be relevant in the initial stages of collagen assembly during tissue morphogenesis, fibrosis, and wound healing.

## SUPPORTING MATERIAL

Supporting data (10 figures with additional data and one Supporting Note explaining the determination of collagen fiber diameter and mass-length ratio by turbidimetry) are available at http://www.biophysj.org/biophysj/supplemental/S0006-3495(13)00619-X.

The authors thank C. Storm, H. Amuasi, B. Meijer, T. de Greef, P. van der Schoot, and B. Mulder for helpful discussions. This work is part of the Industrial Partnership Programme (IPP) Bio(-Related) Materials (BRM) of the Stichting voor Fundamenteel Onderzoek der Materie (FOM), which is financially supported by the Dutch Organization for Scientific Research (NWO). The IPP BRM is cofinanced by the Top Institute Food and Nutrition and the Dutch Polymer Institute.

## REFERENCES

1. Wess, T. J. 2005. Collagen fibril form and function. *Adv. Protein Chem.* 70:341–374.

2. Cox, T. R., and J. T. Erler. 2011. Remodeling and homeostasis of the extracellular matrix: implications for fibrotic diseases and cancer. *Dis. Model. Mech.* 4:165–178.
3. Kadler, K. E., A. Hill, and E. G. Canty-Laird. 2008. Collagen fibrillogenesis: fibronectin, integrins, and minor collagens as organizers and nucleators. *Curr. Opin. Cell Biol.* 20:495–501.
4. Sun, Y. L., Z. P. Luo, …, K. N. An. 2002. Direct quantification of the flexibility of type I collagen monomer. *Biochem. Biophys. Res. Commun.* 295:382–386.
5. Buehler, M. J., and S. Y. Wong. 2007. Entropic elasticity controls nanomechanics of single tropocollagen molecules. *Biophys. J.* 93:37–43.
6. Orgel, J. P., T. C. Irving, …, T. J. Wess. 2006. Microfibrillar structure of type I collagen in situ. *Proc. Natl. Acad. Sci. USA.* 103:9001–9005.
7. Gautieri, A., S. Vesentini, …, M. J. Buehler. 2011. Hierarchical structure and nanomechanics of collagen microfibrils from the atomistic scale up. *Nano Lett.* 11:757–766.
8. Yang, L., K. O. van der Werf, …, M. L. Bennink. 2012. Micromechanical analysis of native and cross-linked collagen type I fibrils supports the existence of microfibrils. *J. Mech. Behav. Biomed. Mater.* 6:148–158.
9. Perumal, S., O. Antipova, and J. P. Orgel. 2008. Collagen fibril architecture, domain organization, and triple-helical conformation govern its proteolysis. *Proc. Natl. Acad. Sci. USA.* 105:2824–2829.
10. Nudelman, F., K. Pieterse, …, N. A. Sommerdijk. 2010. The role of collagen in bone apatite formation in the presence of hydroxyapatite nucleation inhibitors. *Nat. Mater.* 9:1004–1009.
11. Prockop, D. J., and K. I. Kivirikko. 1995. Collagens: molecular biology, diseases, and potentials for therapy. *Annu. Rev. Biochem.* 64:403–434.
12. Eikenberry, E. F., and B. Brodsky. 1980. X-ray diffraction of reconstituted collagen fibers. *J. Mol. Biol.* 144:397–404.
13. Wood, G. C., and M. K. Keech. 1960. The formation of fibrils from collagen solutions. 1. The effect of experimental conditions: kinetic and electron-microscope studies. *Biochem. J.* 75:588–598.
14. Cassel, J., L. Mandelkern, and D. Roberts. 1962. The kinetics of the heat precipitation of collagen. *J. Am. Leather Chem. Assoc.* 57:556–575.
15. Williams, B. R., R. A. Gelman, …, K. A. Piez. 1978. Collagen fibril formation. Optimal in vitro conditions and preliminary kinetic results. *J. Biol. Chem.* 253:6578–6585.
16. Silver, F. H., and D. E. Birk. 1983. Kinetic analysis of collagen fibrillogenesis: I. Use of turbidity—time data. *Coll. Relat. Res.* 3:393–405.
17. Gelman, R. A., B. R. Williams, and K. A. Piez. 1979. Collagen fibril formation. Evidence for a multistep process. *J. Biol. Chem.* 254:180–186.
18. Na, G. C., L. J. Butz, and R. J. Carroll. 1986. Mechanism of in vitro collagen fibril assembly. Kinetic and morphological studies. *J. Biol. Chem.* 261:12290–12299.
19. Na, G. C., L. J. Butz, …, R. J. Carroll. 1986. In vitro collagen fibril assembly in glycerol solution: evidence for a helical cooperative mechanism involving microfibrils. *Biochemistry.* 25:958–966.
20. Na, G. C., L. J. Phillips, and E. I. Freire. 1989. In vitro collagen fibril assembly: thermodynamic studies. *Biochemistry.* 28:7153–7161.
21. Suarez, G., A. L. Oronsky, …, M. H. Koch. 1985. Synchrotron radiation x-ray scattering in the early stages of in vitro collagen fibril formation. *Proc. Natl. Acad. Sci. USA.* 82:4693–4696.
22. Bard, J. B., and J. A. Chapman. 1973. Diameters of collagen fibrils grown in vitro. *Nat. New Biol.* 246:83–84.
23. Gale, M., M. S. Pollanen, …, M. C. Goh. 1995. Sequential assembly of collagen revealed by atomic force microscopy. *Biophys. J.* 68:2124–2128.
24. Cisneros, D. A., C. Hung, …, D. J. Muller. 2006. Observing growth steps of collagen self-assembly by time-lapse high-resolution atomic force microscopy. *J. Struct. Biol.* 154:232–245.
25. Silver, D., J. Miller, …, D. J. Prockop. 1992. Helical model of nucleation and propagation to account for the growth of type I collagen fibrils from symmetrical pointed tips: a special example of self-assembly of rod-like monomers. *Proc. Natl. Acad. Sci. USA.* 89:9860–9864.
26. Gelman, R. A., and K. A. Piez. 1980. Collagen fibril formation in vitro. A quasielastic light-scattering study of early stages. *J. Biol. Chem.* 255:8098–8102.
27. Bernengo, J. C., M. C. Ronziere, …, A. Veis. 1983. A hydrodynamic study of collagen fibrillogenesis by electric birefringence and quasielastic light scattering. *J. Biol. Chem.* 258:1001–1006.
28. George, A., and A. Veis. 1991. FTIRS in H2O demonstrates that collagen monomers undergo a conformational transition prior to thermal self-assembly in vitro. *Biochemistry.* 30:2372–2377.
29. Kasai, M. 1969. Thermodynamical aspect of G-F transformations of actin. *Biochim. Biophys. Acta.* 180:399–409.
30. Gaskin, F., C. R. Cantor, and M. L. Shelanski. 1974. Turbidimetric studies of the in vitro assembly and disassembly of porcine neurotubules. *J. Mol. Biol.* 89:737–755.
31. De Greef, T. F., M. M. Smulders, …, E. W. Meijer. 2009. Supramolecular polymerization. *Chem. Rev.* 109:5687–5754.
32. Kadler, K., Y. Hojima, and D. Prockop. 1987. Assembly of collagen fibrils de novo by cleavage of the type I pC-collagen with procollagen C-proteinase. The jounal of biological chemistry. *J. Biol. Chem.* 260:15696–15701.
33. Streeter, I., and N. H. de Leeuw. 2011. A molecular dynamics study of the interprotein interactions in collagen fibrils. *Soft Matter.* 7:3373–3382.
34. Hulmes, D. J., A. Miller, …, J. Woodhead-Galloway. 1973. Analysis of the primary structure of collagen for the origins of molecular packing. *J. Mol. Biol.* 79:137–148.
35. Traub, W. 1978. Molecular assembly in collagen. *FEBS Lett.* 92:114–120.
36. Leikin, S., D. C. Rau, and V. A. Parsegian. 1994. Direct measurement of forces between self-assembled proteins: temperature-dependent exponential forces between collagen triple helices. *Proc. Natl. Acad. Sci. USA.* 91:276–280.
37. Leikin, S., D. C. Rau, and V. A. Parsegian. 1995. Temperature-favoured assembly of collagen is driven by hydrophilic not hydrophobic interactions. *Nat. Struct. Biol.* 2:205–210.
38. Kar, K., P. Amin, …, B. Brodsky. 2006. Self-association of collagen triple helic peptides into higher order structures. *J. Biol. Chem.* 281:33283–33290.
39. Hayashi, T., and Y. Nagai. 1972. Factors affecting the interactions of collagen molecules as observed by in vitro fibril formation. I. Effects of small molecules, especially saccharides. *J. Biochem.* 72:749–758.
40. Kuznetsova, N., S. L. Chi, and S. Leikin. 1998. Sugars and polyols inhibit fibrillogenesis of type I collagen by disrupting hydrogen-bonded water bridges between the helices. *Biochemistry.* 37:11888–11895.
41. Harris, J. R., and A. Reiber. 2007. Influence of saline and pH on collagen type I fibrillogenesis in vitro: fibril polymorphism and colloidal gold labelling. *Micron.* 38:513–521.
42. Li, Y., A. Asadi, …, E. Douglas. 2009. pH effects on collagen fibrillogenesis in vitro: electrostatic interactions and phosphate binding. *Mater. Sci. Eng. C.* 29:1643–1649.
43. Mertz, E. L., and S. Leikin. 2004. Interactions of inorganic phosphate and sulfate anions with collagen. *Biochemistry.* 43:14901–14912.
44. Prockop, D. J., and A. Fertala. 1998. Inhibition of the self-assembly of collagen I into fibrils with synthetic peptides. Demonstration that assembly is driven by specific binding sites on the monomers. *J. Biol. Chem.* 273:15598–15604.
45. Snowden, J. M., and D. A. Swann. 1979. The formation and thermal stability of in vitro assembled fibrils from acid-soluble and pepsin-treated collagens. *Biochim. Biophys. Acta.* 580:372–381.
46. Gelman, R. A., D. C. Poppke, and K. A. Piez. 1979. Collagen fibril formation in vitro. The role of the nonhelical terminal regions. *J. Biol. Chem.* 254:11741–11745.

47. Helseth, Jr., D. L., and A. Veis. 1981. Collagen self-assembly in vitro. Differentiating specific telopeptide-dependent interactions using selective enzyme modification and the addition of free amino telopeptide. *J. Biol. Chem.* 256:7118–7128.

48. Malone, J. P., and A. Veis. 2004. Heterotrimeric type I collagen C-telopeptideconformation as docked to its helix receptor. *Biochemistry.* 43:15358–15366.

49. Malone, J. P., A. George, and A. Veis. 2004. Type I collagen N-telopeptides adopt an ordered structure when docked to their helix receptor during fibrillogenesis. *Proteins.* 54:206–215.

50. Deshmukh, K., and M. E. Nimni. 1969. Chemical changes associated with aging of collagen in vivo and in vitro. *Biochem. J.* 112:397–405.

51. Na, G. C. 1989. Monomer and oligomer of type I collagen: molecular properties and fibril assembly. *Biochemistry.* 28:7161–7167.

52. Brennan, M., and P. F. Davison. 1980. Role of aldehydes in collagen fibrillogenesis in vitro. *Biopolymers.* 19:1861–1873.

53. Kunii, S., K. Morimoto, …, B. Tonomura. 2010. Actinidain-hydrolyzed type I collagen reveals a crucial amino acid sequence in fibril formation. *J. Biol. Chem.* 285:17465–17470.

54. Marotta, M., and G. Martino. 1985. Sensitive spectrophotometric method for the quantitative estimation of collagen. *Anal. Biochem.* 150:86–90.

55. Carr, Jr., M. E., and J. Hermans. 1978. Size and density of fibrin fibers from turbidity. *Macromolecules.* 11:46–50.

56. Yeromonahos, C., B. Polack, and F. Caton. 2010. Nanostructure of the fibrin clot. *Biophys. J.* 99:2018–2027.

57. Yang, Y.-L., and L. J. Kaufman. 2009. Rheology and confocal reflectance microscopy as probes of mechanical properties and structure during collagen and collagen/hyaluronan self-assembly. *Biophys. J.* 96:1566–1585.

58. Yang, Y.-L., L. M. Leone, and L. J. Kaufman. 2009. Elastic moduli of collagen gels can be predicted from two-dimensional confocal microscopy. *Biophys. J.* 97:2051–2060.

59. Brightman, A. O., B. P. Rajwa, …, S. L. Voytik-Harbin. 2000. Time-lapse confocal reflection microscopy of collagen fibrillogenesis and extracellular matrix assembly in vitro. *Biopolymers.* 54:222–234.

60. Brokaw, J., C. Doillon, …, F. Silver. 1985. Tubridimetry and morphological studies of type I collagen fiber assembly in vitro and the influence of fibronectin. *Int. J. Biol. Macromol.* 7:135–140.

61. Piechocka, I. K., A. S. van Oosten, …, G. H. Koenderink. 2011. Rheology of heterotypic collagen networks. *Biomacromolecules.* 12:2797–2805.

62. Wang, Y., J. Silvent, …, M. Giraud Gille. 2011. Controlled collagen assembly to build dense tissue-like materials for tissue engineering. *Soft Matter.* 7:11203–11210.

63. Strasser, S., A. Zink, …, S. Thalhammer. 2007. Structural investigations on native collagen type I fibrils using AFM. *Biochem. Biophys. Res. Commun.* 354:27–32.

64. Grant, C. A., D. J. Brockwell, …, N. H. Thomson. 2009. Tuning the elastic modulus of hydrated collagen fibrils. *Biophys. J.* 97:2985–2992.

65. Jiang, F., H. Hörber, …, D. J. Müller. 2004. Assembly of collagen into microribbons: effects of pH and electrolytes. *J. Struct. Biol.* 148:268–278.

66. Stein, M., D. Vader, …, L. Sander. 2011. The micromechanics of three-dimensional collagen-I gels. *Complexity.* 16:22–28.

67. Motte, S., and L. J. Kaufman. 2013. Strain stiffening in collagen I networks. *Biopolymers.* 99:35–46.

68. Lindström, S. B., D. A. Vader, …, D. A. Weitz. 2010. Biopolymer network geometries: characterization, regeneration, and elastic properties. *Phys. Rev. E Stat. Nonlin. Soft Matter Phys.* 82:051905.

69. Broedersz, C. P., M. Sheinman, and F. C. Mackintosh. 2012. Filament-length-controlled elasticity in 3D fiber networks. *Phys. Rev. Lett.* 108:078102.

70. Ayad, S., and C. H. Wynn. 1970. The effect of semicarbazide on the nature and stability of collagen fibrils. *Biochem. J.* 118:61–65.

71. Tanzer, M. L. 1968. Intermolecular cross-links in reconstituted collagen fibrils. Evidence for the nature of the covalent bonds. *J. Biol. Chem.* 243:4045–4054.

72. Payne, K. J., T. A. King, and D. F. Holmes. 1986. Collagen fibrillogenesis in vitro: an investigation of the thermal memory effect and of the early events occurring during fibril assembly using dynamic light scattering. *Biopolymers.* 25:1185–1207.

73. Hayashi, T., and Y. Nagai. 1974. Time-dependent increase in stability of collagen fibrils formed in vitro. Effect of temperature. *J. Biochem.* 75:651–654.

74. Hayashi, T. 1978. Time-dependent increase in the stability of collagen fibrils formed in vitro. I. Effects of pH and salt concentration on the dissolution of the fibrils. *J. Biochem.* 84:245–249.

75. Kueh, H. Y., W. M. Brieher, and T. J. Mitchison. 2008. Dynamic stabilization of actin filaments. *Proc. Natl. Acad. Sci. USA.* 105:16531–16536.

76. Kueh, H. Y., and T. J. Mitchison. 2009. Structural plasticity in actin and tubulin polymer dynamics. *Science.* 325:960–963.

77. Niedermayer, T., A. Jégou, …, R. Lipowsky. 2012. Intermittent depolymerization of actin filaments is caused by photo-induced dimerization of actin protomers. *Proc. Natl. Acad. Sci. USA.* 109:10769–10774.

78. Hulmes, D. J., T. J. Wess, …, P. Fratzl. 1995. Radial packing, order, and disorder in collagen fibrils. *Biophys. J.* 68:1661–1670.

79. Hulmes, D. J., J. C. Jesior, …, C. Wolff. 1981. Electron microscopy shows periodic structure in collagen fibril cross sections. *Proc. Natl. Acad. Sci. USA.* 78:3567–3571.

80. Schoenenberger, C. A., S. Buchmeier, …, B. M. Jockusch. 2005. Conformation-specific antibodies reveal distinct actin structures in the nucleus and the cytoplasm. *J. Struct. Biol.* 152:157–168.

81. Dimitrov, A., M. Quesnoit, …, F. Perez. 2008. Detection of GTP-tubulin conformation in vivo reveals a role for GTP remnants in microtubule rescues. *Science.* 322:1353–1356.

82. Amuasi, H. E., and C. Storm. 2010. Off-lattice Monte Carlo simulation of supramolecular polymer architectures. *Phys. Rev. Lett.* 105:248105.

83. Maggs, A., D. Huse, and S. Leibler. 1989. Unbinding transitions of semi-flexible polymers. *Europhys. Lett.* 8:615–620.

84. Benetatos, P., and E. Frey. 2003. Depinning of semiflexible polymers. *Phys. Rev. E Stat. Nonlin. Soft Matter Phys.* 67:051108.

85. Kierfeld, J. 2006. Force-induced desorption and unzipping of semiflexible polymers. *Phys. Rev. Lett.* 97:058302.

86. Hirshburg, J. M., K. M. Ravikumar, …, A. T. Yeh. 2010. Molecular basis for optical clearing of collagenous tissues. *J. Biomed. Opt.* 15:055002.

87. Pachence, J. M. 1996. Collagen-based devices for soft tissue repair. *J. Biomed. Mater. Res.* 33:35–40.

**Supporting Material**

# Thermal Memory in Self-assembled Collagen Fibril Networks

Martijn de Wild, Wim Pomp, and Gijsje H. Koenderink*
Biological Soft Matter Group, FOM Institute AMOLF, Science Park 104,
1098 XG Amsterdam, the Netherlands

Address reprint requests and inquiries to Gijsje H. Koenderink, Email: g.koenderink@amolf.nl

## Note S1. Determination of collagen fiber diameter and mass-length ratio by turbidimetry

The wavelength dependence of the turbidity of a solution of rigid fibers contains information about the fiber diameter, $d$, and their mass-length ratio, $\mu$. The exact functional dependence is model-dependent. Assuming that the fibers are randomly oriented, rigid rod-like, and monodisperse in size, the turbidity scales with wavelength as (1, 2):

$$\tau\lambda^5 = A\mu(\lambda^2 - Bd^2) \qquad (1)$$

This relation is valid when the rods are longer than ~800 nm and have a diameter less than ~200 nm (2). According to Eq. (1), $d$ and $\mu$ can be simply determined by plotting $\tau\lambda^5$ versus $\lambda^2$. The mass-length ratio, $\mu$, follows from the slope of this linear relation, using the definition $A = (88/15)\pi^3 c n_s (dn/dc) 21/N_A$, where $c$ is the protein concentration expressed in g ml$^{-1}$, $n_s$ is the solvent refractive index (equal to 1.33), $dn/dc$ is the specific refractive index increment ($dn/dc$ = 0.186 cm$^3$ g$^{-1}$ for collagen(3)), and $N_A$ is Avogadro's constant. The fiber diameter $d$ can be calculated by combining the measured intercept with the y-axis ($-A\mu Bd^2$) with the measured slope, using the definition $B = (92/426)\,\pi^2 n_s^2$.

We measured $d$ and $\mu$ for collagen solutions during polymerization at 37°C by measuring the wavelength dependence of the turbidity at 8 evenly spaced wavelengths between 370 and 440 nm, using time intervals of 2 minutes between consecutive wavelength scans. For all wavelengths, the turbidity remained essentially zero during the first 15 minutes of assembly, indicative of a lag phase during which fibrils are nucleated. During this nucleation phase, we were thus unable to reliably track the fiber diameter and mass. After 15 minutes, the turbidity at each wavelength increased sigmoidally with time, indicating fiber growth. The wavelength dependence of the turbidity obeyed the linear scaling predicted by Eq. (1), consistent with the presence of rigid, high aspect ratio fibrils. The slope $A\mu$ increased over time, indicating that the fibrils grow laterally (Fig. S1). After 2 hours incubation at 37°C, we suddenly lowered the temperature to a value between 4 and 32°C in order to induce fibril disassembly. In response, both the magnitude of the turbidity and the slope $A\mu$ decreased, indicating that fibrils loose monomers from their sides (Fig. S1, solid red circles).

As shown in Fig. S2a (left hand side), the apparent mass length ratio of the fibrils increased in a sigmoidal fashion during the growth phase. At the end of the lag phase, the mass-length ratio was about $1.3.10^{12}$ Da.cm. Given a quarter-staggered axial packing of collagen molecules with a period of $D$ = 67.2 nm, the number of molecules per fibril cross-section is $N = \mu/(M^*4.6D)$, where $M$ is the molecular mass of collagen (290 kDa(4)). At the end of the turbidimetric growth phase, the fibrils thus have ~130 monomers per cross-section, consistent with prior reports (5, 6). The final mass length ratio of "mature collagen fibrils" formed after 2 hours at 37°C was $1.03.10^{13}$ Da/cm with a standard deviation of 7% ($N$

= 6), corresponding to an average of 1070 monomers per cross-section. These values are closely comparable to those measured for collagen fibrils formed at 37°C from purified rat tail collagen I (7).

Upon cooling, the mass-length ratio decreased in a bi-phasic manner, showing an initial fast decay followed by a slow decay that was incomplete even after 2 hours (Fig. S2a, right hand side). The loss of mass from the sides was strongly temperature dependent. At the lowest temperature (4°C), the final mass length ratio was $2.2.10^{12}$, corresponding to 229 monomers per fibril cross-section.

The apparent fibril diameter started at a value of about 20 nm at the end of the lag phase, and increased to values ranging between 42 and 70 nm after 2 hours assembly at 37°C (Fig. S2b). The average diameter of "mature fibrils" was 61 nm with a standard deviation of 22%. Upon cooling, the apparent diameter, surprisingly, jumped up to higher values (80-100 nm) and afterwards showed a biphasic decay which was often rather noisy (see for instance the 4°C trace in Fig. S2b). We currently have no definitive interpretation of this behavior, but we strongly suspect that the diameter measurements are prone to artifacts, since the sudden jump upon cooling is clearly unphysical. We suspect that the diameter measurements are fundamentally inaccurate because the diameters are about 10-fold smaller than the wavelengths used; as a result, the extrapolation required to measure the y-intercept of $\tau\lambda^5$ versus $\lambda^2$ curves becomes very inaccurate. We nevertheless expect that the measured values of $\mu$ are reasonable, since light scattering theories predict that $\mu$ can still be determined from the slope in the limit of fibrils much thinner than $\lambda$ (1).

We can compare the reduction of $\mu$ as a function of disassembly temperature ($\mu_{dis}/\mu_{37}$) with the reduction of turbidity ($\tau_{dis}/\tau_{37}$). The latter quantity provides a model-independent measure of the overall loss in fibril mass. As shown in Fig. S4, $\mu_{dis}/\mu_{37}$ is nearly identical to $\tau_{dis}/\tau_{37}$ over the entire range of disassembly temperatures, strongly suggesting that fibrils mainly loose mass from their sides. We observe that $\mu_{dis}/\mu_{37}$ is consistently somewhat larger than $\tau_{dis}/\tau_{37}$, which is consistent with mass being lost also from the fibril ends. This in turn is consistent with confocal microscopy data, showing that cooling promotes the formation of dangling ends.

**Supporting References (References also appear in the Main Text)**

1) Carr, M., and J. Hermans. 1978. Size and density of fibrin fibers from turbidity. *Macromolecules*. 11: 46-50.
2) Yeramonahos, C., B. Polack, and F. Caton. 2010. Nanostructure of the fibrin clot. *Biophys. J.* 99: 2018-2027.
3) Brokaw, J., C. Doillon, R. Hahn, D. Birk, R. Berg, and F. Silver. 1985. Turbidimetry and morphological studies of type I collagen fiber assembly in vitro and the influence of fibronectin. *Int. J. Biol. Macromol.* 7: 135-140.
4) Wess, T. 2005. Collagen fibril form and function. *Adv. Protein Chem.* 2005: 341 - 374.
5) Bard, J., and J. Chapman. 1973. Diameters of collagen fibrils grown in vitro. *Nat. New Biol.* 246: 83 - 84.
6) Silver, F., and D. Birk. 1983. Kinetic analysis of collagen fibrillogenesis: I. Use of turbidity--time data. *Coll. Relat. Res.* 3: 393 - 405
7) Piechocka, I., A. VanOosten, R. Breuls, and G. Koenderink. 2011. Rheology of heterotypic collagen networks. *Biomacromolecules*. 12: 2797-2805.

**Supplemental Figures**

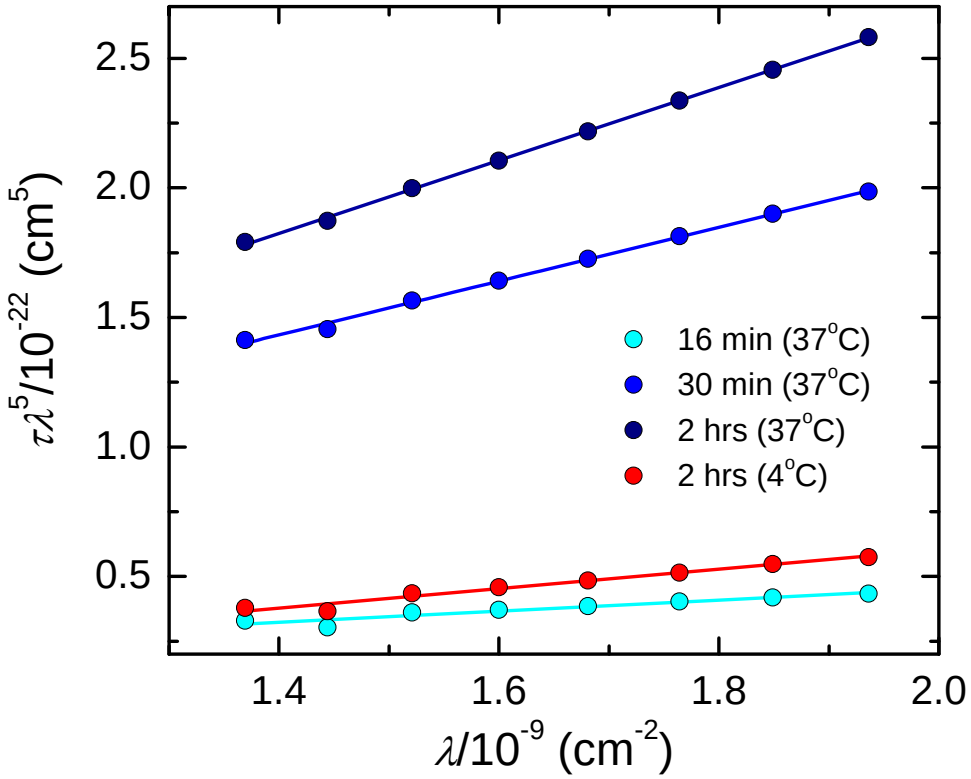


Supplemental Figure S1. **Wavelength dependence of the turbidity of a 1 mg/ml collagen gel, plotted according to Eq. 1 in Supporting Note S1.** The plots are linear, consistent with the presence of long, thin fibers (lines are best fits to the data). Three of the measurements shown were obtained at different times during fibril assembly at 37°C (16, 30, 120 minutes after induction of polymerization by warming from 4 to 37°C); fibril polymerization is evident from the increase in the magnitude of the turbidity and in the increase of the slope. One measurements was obtained after disassembly of the gel for 2 hours at 4°C (see figure legend); disassembly is evident from the decrease of the turbidity and the decrease of the slope.

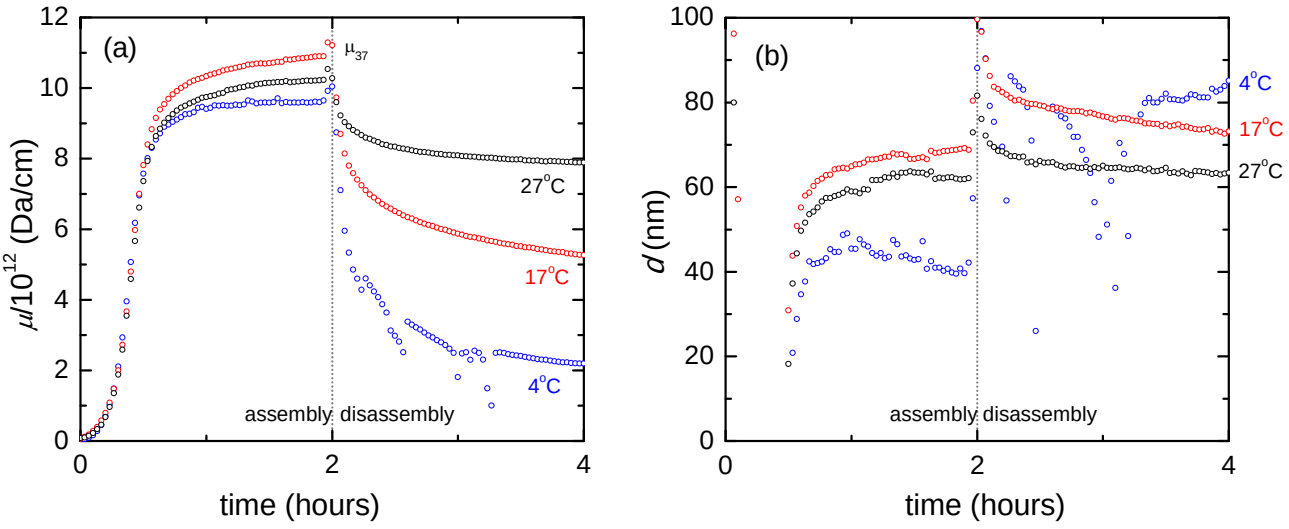


Supplemental Figure S2. **Structural properties of collagen fibrils during assembly and disassembly, as determined from the wavelength dependence of the turbidity.** (a) Fibril mass-length ratio and (b) fibril diameter, shown as a function of time during fibril assembly at 37°C for 2 hours (left of dashed vertical lines) and during fibril disassembly triggered by stepwise cooling to 4, 17, or 27°C**.** The analysis of the data assumes that the fibrils are long, thin, rigid, monodisperse, and randomly oriented, as explained in Supporting Note S1.

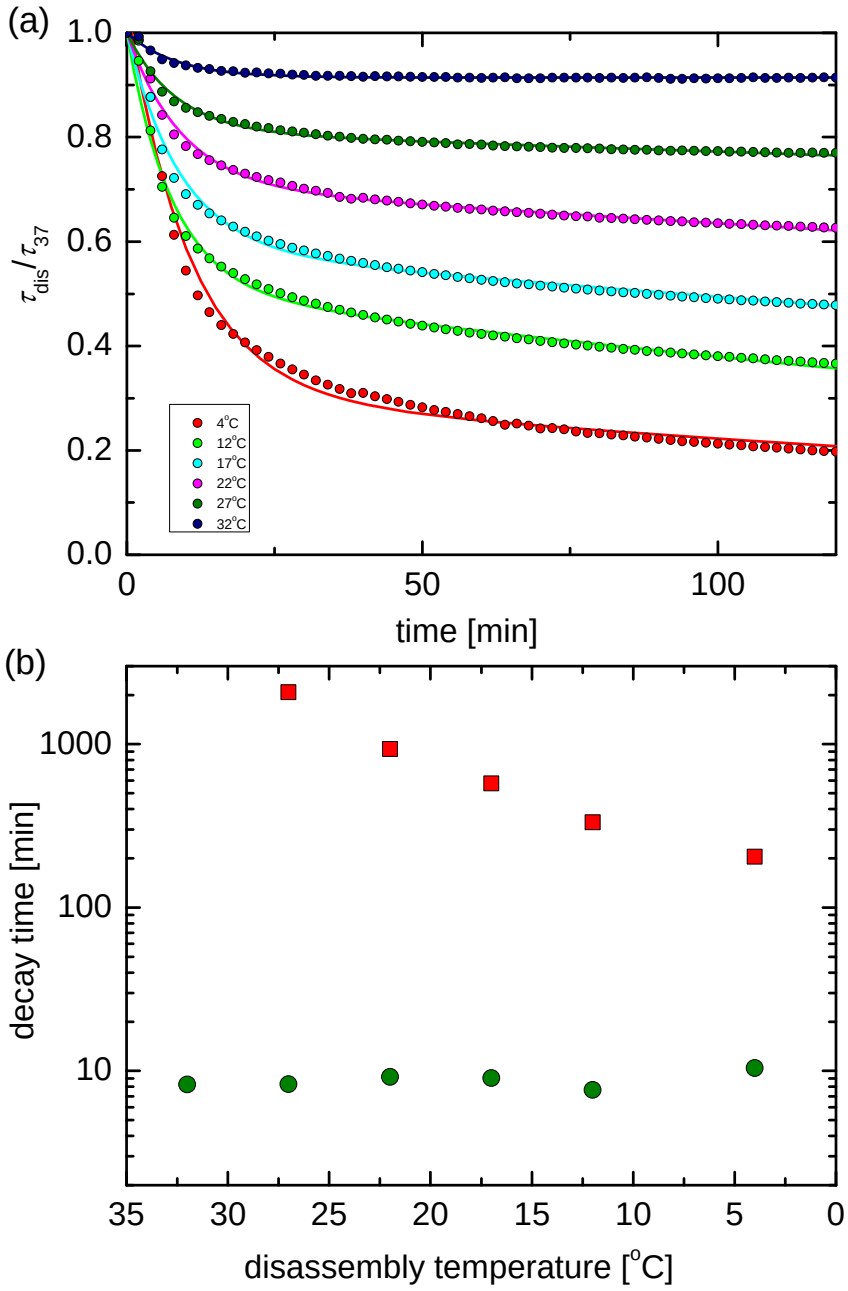


Supplemental Figure S3. **Empirical double-exponential fits to the time-dependent decay of the turbidity measured upon sudden cooling of collagen gels formed for 2 hours at 37°C.** The turbidity is normalized by the turbidity of the "mature collagen fibrils" (formed after 2 hours incubation at 37°C), according to $\tau_{dis}/\tau_{37}$. The fitting formula was: $\tau_{dis}/\tau_{37} = P_{fast} \exp(-t/ t_{fast}) + P_{slow} \exp(-t/t_{slow})$ with the constraint that $P_{fast} + P_{slow} = 1$. (a) Example data sets (symbols) with double-exponential fits (lines). (b) Dependence of the two decay times, $t_{fast}$ and $t_{slow}$, on disassembly temperature. The fast decay time is temperature-independent. The slow time scale increases strongly with increasing disassembly temperature; at 32°C, $t_{slow}$ diverges. The fraction of the fast-decaying component is 65% at 4°C, 49% at 12°C, 41% at 17°C, 29% at 22°C, 19% at 27°C, and 10% at 32°C.

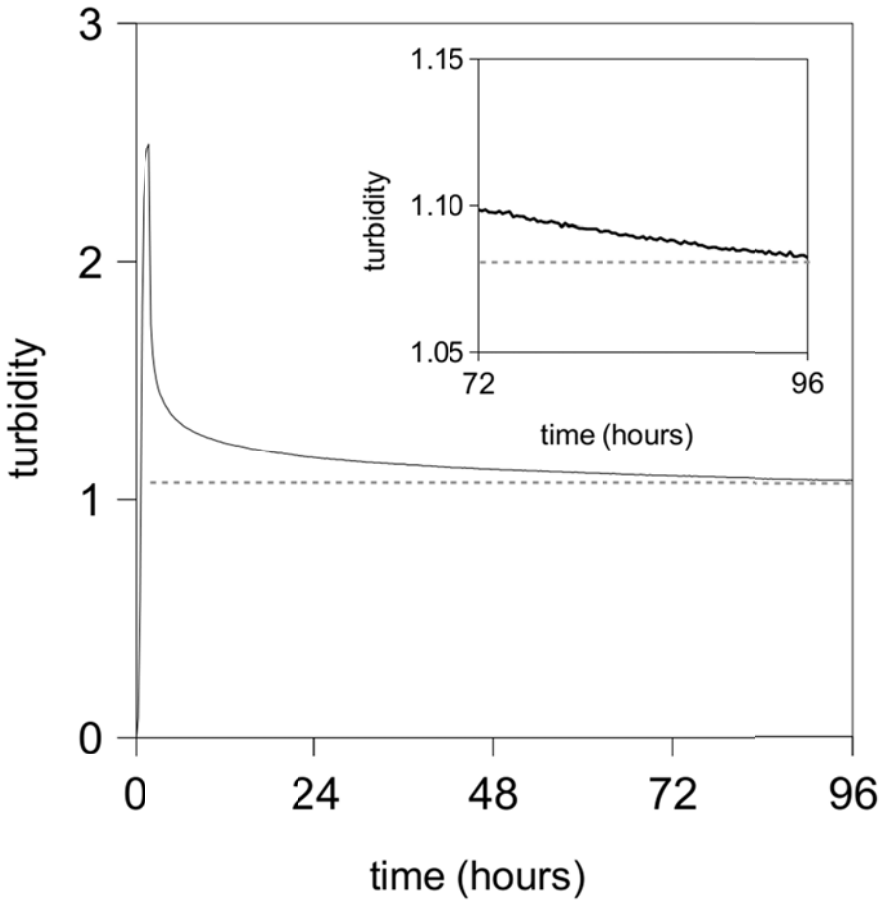


Supplemental Figure S4. **The turbidity of a 1 mg/ml collagen gel as a function of time.** After assembly at 37°C for 2 hours, the temperature is abruptly lowered to 22°C. Even after 96 hours, the turbidity is still slowly decreasing with time, which is more obvious in the *Inset*, which shows the same data, but zoomed in on the last 24 hours. The horizontal dotted lines are added to guide the eye.

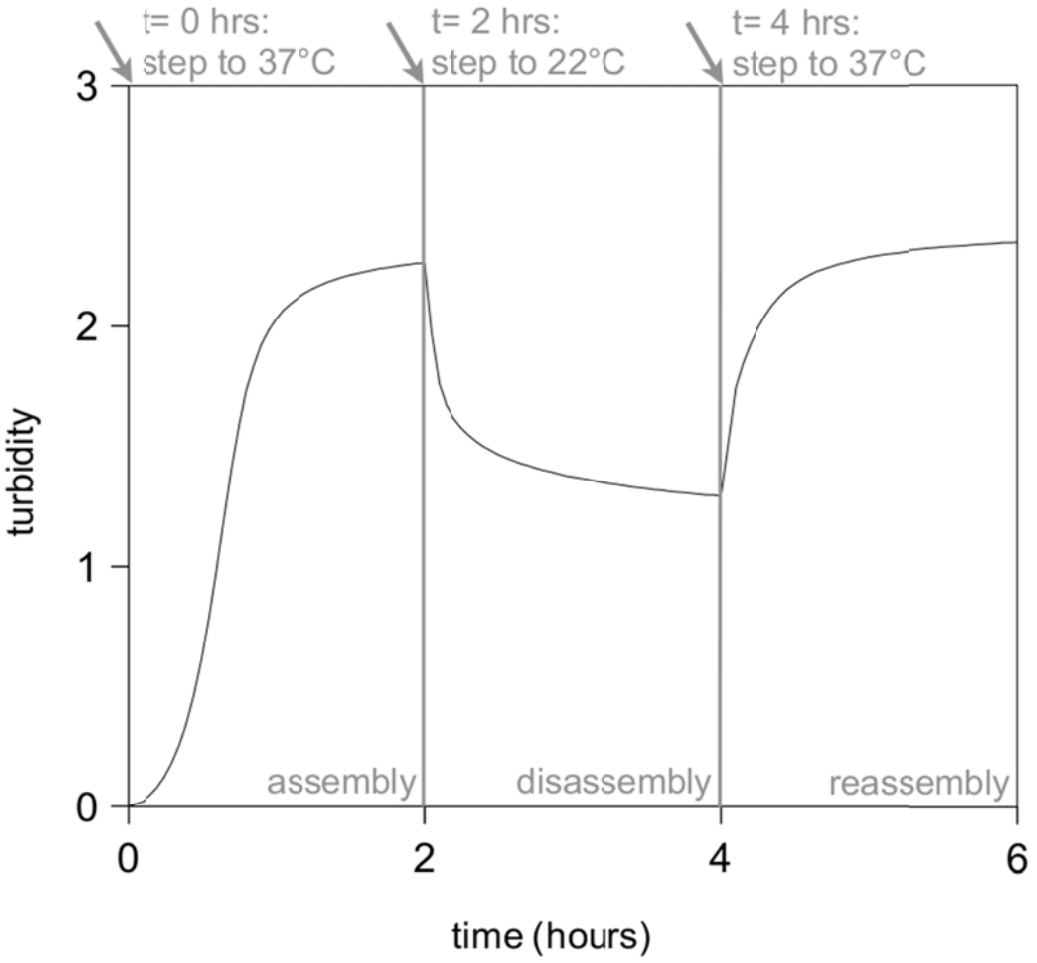


Supplemental Figure S5. **The turbidity of a 1 mg/ml collagen gel as a function of time.** After the 2 hours needed for assembly at 37°C, the temperature is lowered to 22°C, stepwise. After 2 hours of disassembly, it is raised again to 37°C, stepwise.

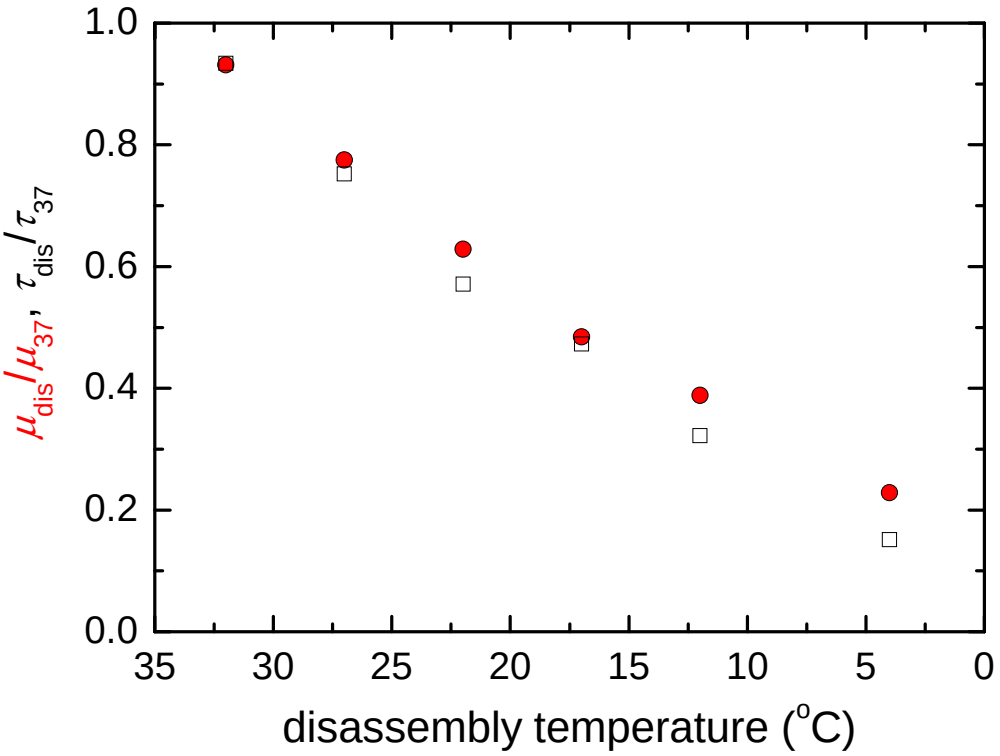


Supplemental Figure S6. **Comparison between the temperature dependence of the loss in fibril mass-length ratio ($\mu_{dis}/\mu_{37}$, solid red circles) determined by analyzing the wavelength dependence of the turbidity (which is model-dependent, see Supporting Note S1), with the loss in fibril mass** as quantified in a model-independent manner from the relative change in turbidity measured at a single wavelength of 370 nm ($\tau_{dis}/\tau_{37}$, open black squares)**.** The two measures are comparable, which suggests that mass is predominantly lost from the sides.

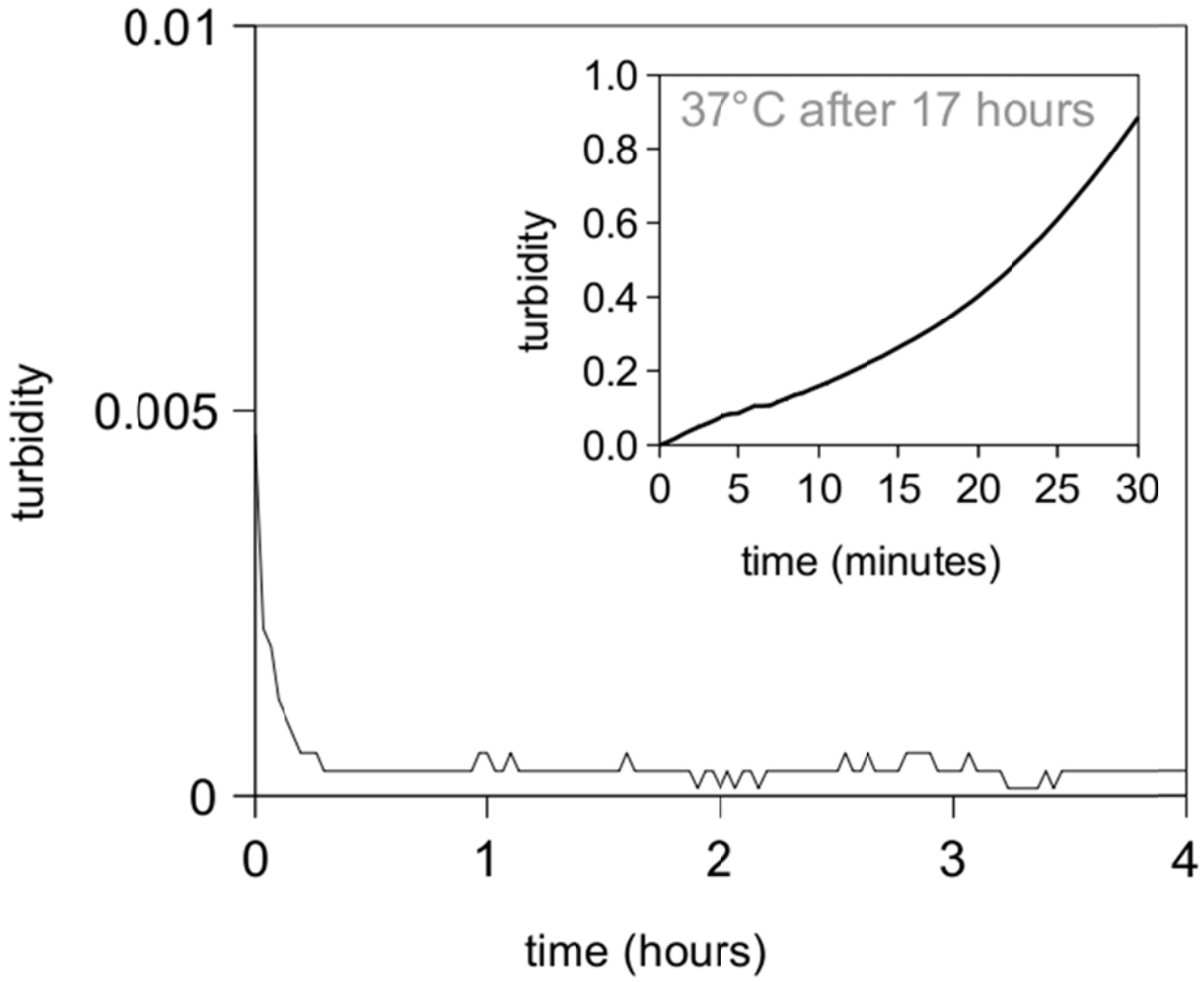


Supplemental Figure S7. **The turbidity of a 1 mg/ml collagen solution, kept at 4°C, as a function of time.** No appreciable turbidity develops, indicating that no fibril assembly takes place. The slightly higher value around $t = 0$ is an artefact common to these experiments. *Inset*: after 17 hours at 4°C, the temperature is increased stepwise to 37°C, causing an immediate increase in turbidity.

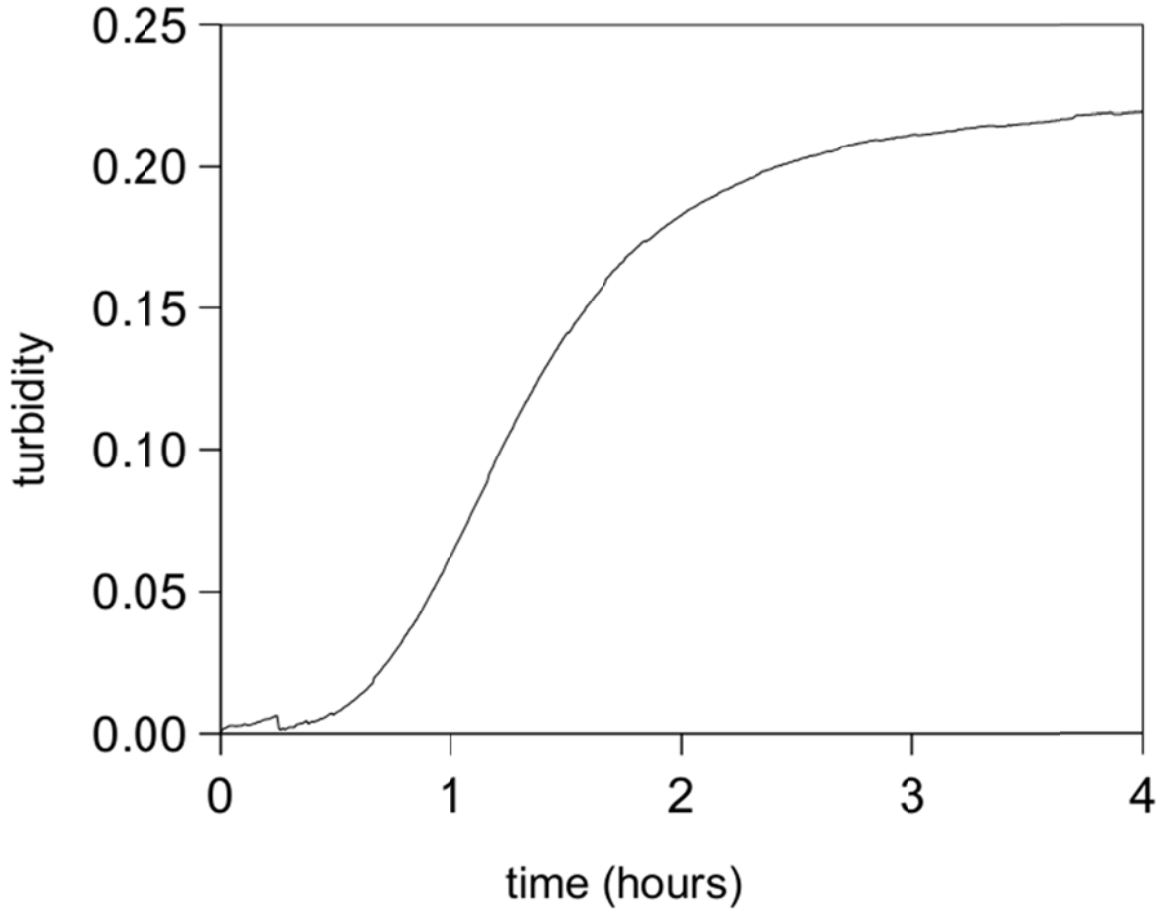


Supplemental Figure S8. **Turbidity as a function of time of a 0.1 mg/ml collagen gel.** The collagen used in this mixture is prepared by assembling a 1.0 mg/ml gel, and then redissolving it in 0.01M HCl at 4°C. There is a lag phase of approximately 30 minutes, indicating that the redissolved collagen solution contains no nuclei or other supramolecular aggregates. The experiment was performed by assembling fibrils inside a dialysis cartridge (Slide-a-lyzer, 30,000 MWCO, 0.5-3ml capacity, Thermo Scientific) pre-soaked in assembly buffer. After 2 hours of assembly, the gel was dialysed against 3 changes of 150 ml 0.01M HCl at 4°C. The collagen solution was then re-assembled by adding assembly buffer, adjusting the pH to 7.2, and raising the temperature to 37°C. Assembly was monitored by turbidimetry.

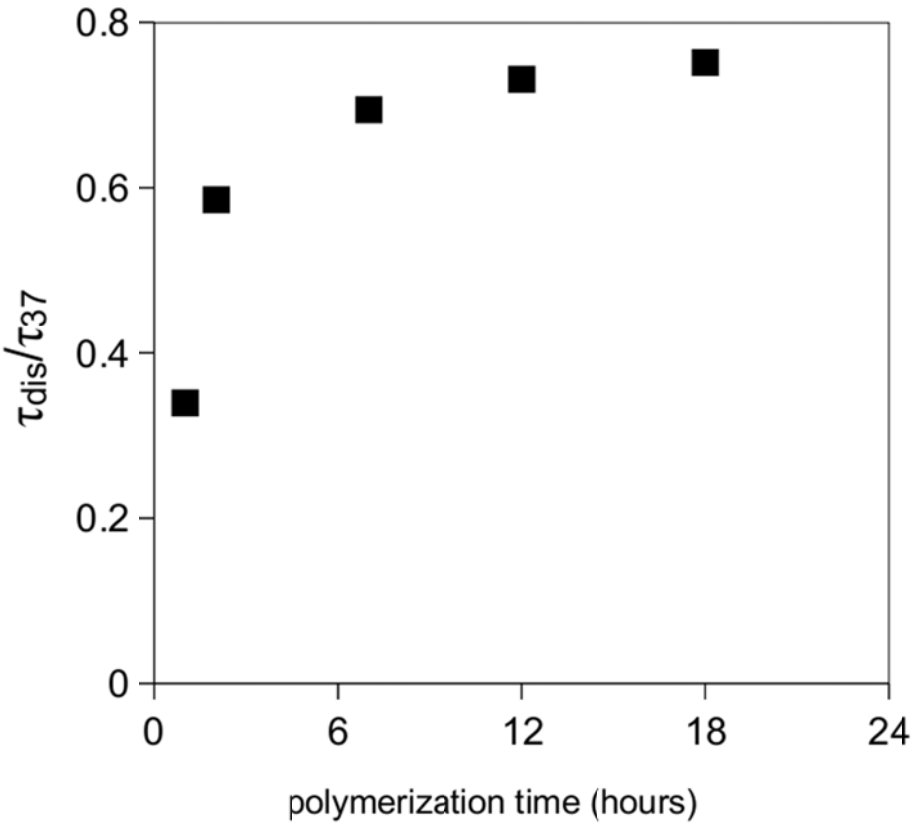


Supplemental Figure S9. **Age-dependence of fibril disassembly.** $\tau_{dis}/\tau_{37}$ measured 2 hours after a temperature step to 22°C, as a function of the polymerization time.

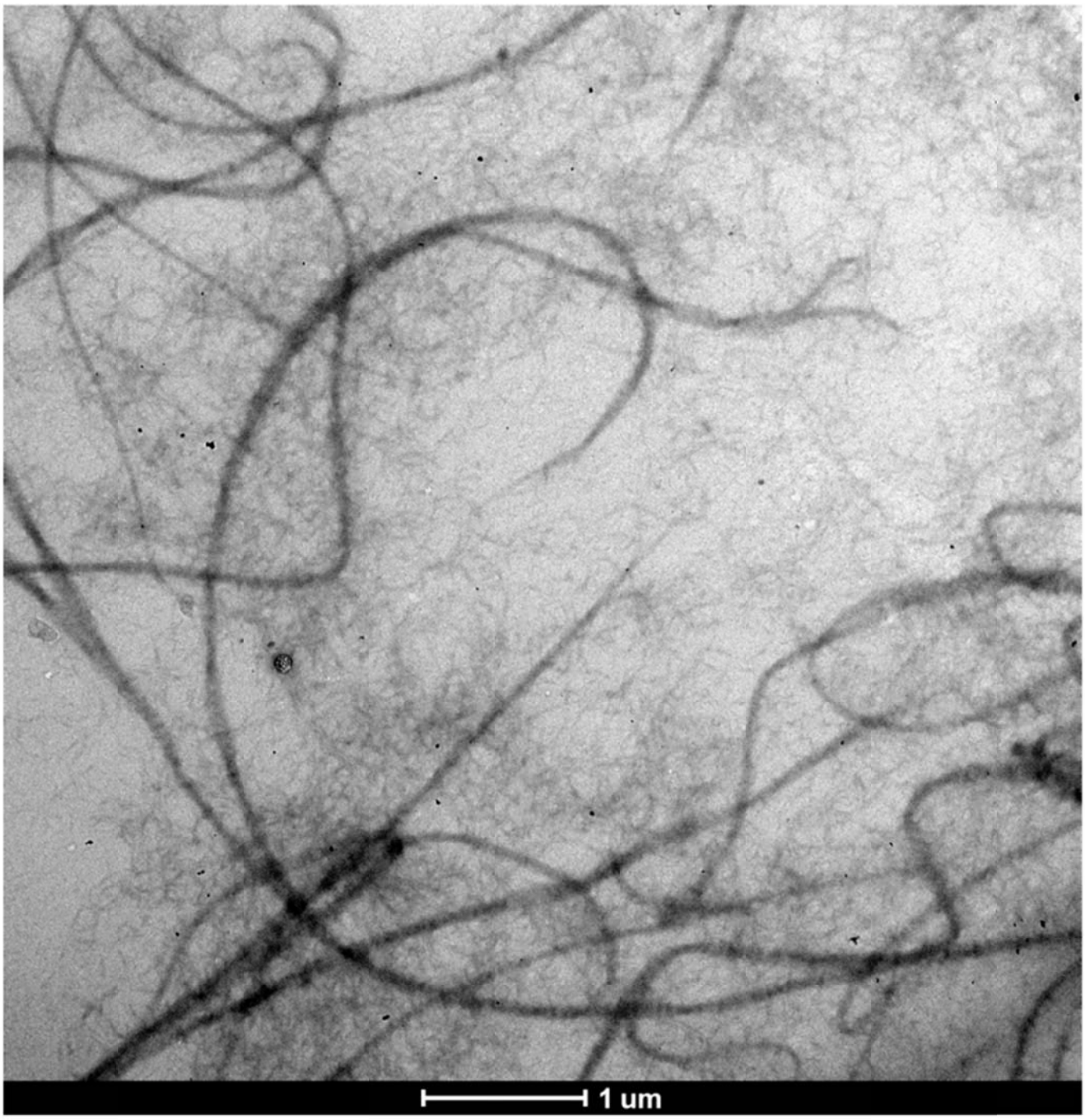


Supplemental Figure S10: **Transmission electron microscopy image of collagen fibrils from a 0.25 mg/ml gel.** The fibrils were formed at 37°C for 2 hours, and then disassembled at 22°C for 2 hours.